UNIVERSIDAD DE CONCEPCIÓN
FACULTAD DE CIENCIAS FÍSICAS Y MATEMÁTICAS
MAGÍSTER EN ASTRONOMÍA

Unveiling NH_3 Depletion in Pre-Stellar Cores

Revelando el Agotamiento del NH3 en los Núcleos Preestelares

Autor:
Daniel Gaete Espinoza

Profesor Guía:
Dr. Stefano Bovino

Comisión:
Dominik Schleicher, Alessandro Lupi & Rodrigo Reeves

Tesis para ser presentada a la Dirección de Postgrado de la Universidad de Concepción para optar al grado académico de Magíster en Astronomía

CONCEPCIÓN, CHILE
2023

Unveiling NH_3 Depletion in Pre-Stellar Cores

Abstract

Molecular clouds are regions in the interstellar medium where molecular H_2 lies and accumulates. When the concentration of molecular hydrogen becomes high enough, the properties of the region that contains it begin to change, preparing it for the collapse that, with enough evolution, will form new stars. These high-density regions are normally known as Cores, receiving a name depending on their state of evolution, starting from starless cores where there is a clear over-density but no gravitational bonding, to pre-stellar cores, where gravity plays an important role in the core dynamics. Pre-stellar cores have been extensively studied and recognized for having very special chemical traits that are expected to determine the future of the stars that will be born from them. In these terms, one specific and important property of pre-stellar cores is the high level of depletion of heavy species into dust grain surfaces. Ammonia (NH_3) had been flying under the radar for more than a decade because, as observed in some observational projects, it does not freeze out as hard or at all as C and O-based molecules. In this work, we study the creation and evolution of NH_3, its deuterated isotopologues, and spin isomers, making use of up-to-date chemical post-processing over the results of a state-of-art 3D hydrodynamic numerical simulation. We used this chemical post-processing scheme to see how changing some parameters affects the behavior of NH_3 on an evolving slow collapse pre-stellar core and compared the results to observations. We find that a high value of CRIR, even if that is quite difficult under pre-stellar core conditions, can increase NH_3 abundance and decrease the effects of freeze-out over it, while smaller grain sizes and high ortho-para ratios promote depletion heavily. We also explore the effects of implementing a density dependence for gas and dust temperatures and CRIR, which showed slight improvements from the worst isothermal cases; in particular, in the density-dependent CRIR case, we got results close to the best regular cases. We then compare our findings, mostly qualitatively, with a couple of more up-to-date observational works than our reference one, probing that our post-processing scheme, both in isothermal and density-dependent cases, can roughly recover the observed column densities on these publications, which validates our approach. We conclude that most of the parameters we have explored have a relatively weak role when we talk about regulating ammonia depletion, but there are some exceptions, as is the case when CRIR is high. Also, we find that our fiducial run does not have the best agreement with the reference case as we expected when contrasting them all, but its abundance profile is congruent with the observations over the whole evolutionary process.

Acknowledgements

When I think of acknowledgements, even if I want to thank a lot of people, I admit that I do not know where to start, but it is something that must be done, because I am really grateful for a lot of things.

First, I want to thank my family, especially my mother, sister, and mother's side grandparents, for supporting me in their own way, even if I did not look totally sure about following a scientific career, and for letting me make mistakes so I could learn for myself how life works and how to build my own path in this world.

Second, I want to thank my secondary school math, physics, and arts professors, as they were really supportive of me and gave me a great impulse to go this way, which will meet its first end with this thesis.

Also, I'd like to thank all of the friends I've met and made at university for making this journey called studying a major a lot more comfortable, and some of them have also reunited me with my trust in others, which I thought I'd lost a long time ago, and demonstrated that I could also be a sociable guy.

In addition to all the previous acknowledgements, I would like to thank all the professors I had classes with at the university, even if I did not get the best results on their respective subjects, because, one way or another, I learned a lot from them.

I would especially like to thank all of the members of this thesis revisor committee, as they will be the ones who allow me to move forward. Also, I would like to thank my first supervisor, Amelia Stutz. Even if things between us didn't go well, she gave me the minimum grade required to have another opportunity, which led finally to this thesis.

And last, but not least, I want to thank my thesis supervisor, Stefano Bovino, for taking me when I was about to lose the Masters, close to giving up on my goals and dreams, giving me an opportunity to start again, another opportunity to try to become what I wanted, believing in me and supporting me even in the worst situations. I know I was not the best student for him and that I did a lot of things wrong, but he didn't lose hope. I will always be in debt to him.

I want to finalize these acknowledgements with a personal phrase that I said randomly to someone a while ago trying to cheer them up and that nowadays represents the way I like to see this crazy ride we humans call life:

"Think of life as an hourglass; if there is still sand inside the hourglass, if there is life, we can start over again."

Contents

List of Figures

List of Tables

Chapter 1

Introduction

Astronomy is the science that studies the cosmos as a whole, from the biggest galaxy clusters on the macro side to the behavior of particles and molecules out of earth's atmosphere conditions on the micro side. Between the vast range of topics and objects that astronomy covers, stars are, without doubt, the most important, or at least the most covered, among all of them. The reasons why stars are important in astronomy are quite numerous, but, for this work, the main reason is that, over their lives, from birth to death, they have a notable impact on the chemical features of their environment, enriching and reorganizing it. How important is the impact of a specific star on the chemistry of its surroundings? It is primarily (and only if no catastrophic events occur) determined by the mass it had at its birth, during star formation.

Star formation is a well-studied yet not completely understood process that occurs in regions known as molecular clouds, which are, in simple terms, great concentrations of molecular hydrogen in relatively compact zones of space. While the composition of these structures is pretty simple, the star formation process as a whole is quite complex, especially as several physical conditions must be met to trigger it, and the results will vary depending on the said conditions. Some substructures of molecular clouds, known as pre-stellar cores, concentrate interstellar matter on them before stars form. Their peculiar conditions give rise to several characteristic chains of reactions that, in turn, give shape to their chemical structure on a well-known level.

Over the last decades, several studies have revealed the chemical complexity of pre-stellar cores and the new chemical processes they reveal. A high abundance of ammonia NH_3 has been found in the central parts of pre-stellar cores, which is a very distinct feature. This molecule was first documented to be present in the Interstellar Medium (ISM) by Cheung et al. (1968). It has since been discovered to be abundant in almost all parts of the ISM in almost all types of environments. Due to its spectroscopic features, interstellar NH_3 has been used as a thermometer to keep track of the kinetic temperature of the gas where it is located (Crapsi et al., 2007), while also being used as a probe in the densest regions inside molecular clouds (Tafalla et al. 2004,Ho and Townes 1983).

As ammonia is a molecular species heavier than helium, it is expected to show a decrease in its abundance when it is measured towards the center of pre-stellar cores, as it happens with C and/or O-bearing molecules, via the well-known process called freeze-out. However, contrary to what astrochemical one-zone models predicted (Sipilä et al., 2015; Sipilä et al., 2019), ammonia has been observed in several cases to have an excess in the gas-phase (see Flower et al., 2006, and references therein), with a tendency to maintain or even increase it when moving to denser regions (Tafalla et al., 2004; Crapsi et al., 2007), where it is supposed to be depleted.

With no definitive solution yet, this inconsistency between models and observations, or even between different observations, has raised the question of what the main formation path for ammonia in dense clouds is. On the one hand, gas-phase synthesis of ammonia is well-known to start with either: i) the dominant $N^+ + H_2$ reaction, or ii) the $N + H_3^+$ reaction; both followed by hydrogen abstractions, and dissociative recombination (DR) reactions (Herbst et al., 1987; Scott et al., 1997). This path was long thought to be efficient enough to reproduce the observed abundances (Le Bourlot, 1991a). However, in a recent work Le Bourlot (1991b) re-examined the $N^+ + H_2$ reaction rate, finding a meaningfully lower value, well below the one obtained by Herbst et al. (1987) to explain the observed abundances of ammonia. Moreover, its formation on the surface of interstellar dust grains via successive hydrogenation of a single nitrogen atom (Hidaka et al., 2011; Fedoseev et al., 2015) remains unconstrained. Particularly, how much ammonia is desorbed from the grain surface and what the main desorption mechanism is remain unknown (Sipilä et al., 2019). Thus, the relative importance of the formation of ammonia between the gas phase and that happening on grain surfaces remains a conundrum (see Le Gal et al., 2014, and references therein).

The goal of this thesis is to better understand the behavior of ammonia in pre-stellar core conditions and its importance in the understanding of the star-formation process. The thesis is organized as follows: In Chapter 2, we define the interstellar medium and introduce the properties of its densest and coldest regions, which are the focus of this work. In Chapter 3 we review how chemistry works in star-forming regions and how this affects ammonia. In Chapter 4 we describe the chemical post-processing method we used and the modifications we made for this work. In Chapter 5 we show the different results we got and discuss the discrepancies between them and recent works. Finally, in Chapter 6, we summarize our results and propose some prospects.

Chapter 2

Astrophysical context

In this chapter, we shall introduce the environment and the conditions that affect the chemical processes involving ammonia. We will present a brief description of our Galaxy interstellar medium, discussing the processes occurring at small scales, and then give a review of the associated chemistry in Chapter 3.

2.1 The Interstellar Medium

Although there are some astronomical topics that can be investigated during daylight, as is the case with our nearest star, the Sun, most observations here on Earth must be done during the night, at least in the optical and ultraviolet (UV) bands. Between all objects visible only during the dark hours of the night, it is clear that stars do captivate our attention first, as they shine in the middle of darkness. Even though those *sky lights* may appear to be the only thing out there, we can find several other kinds of objects in outer space, such as charged particles, interstellar dust, gas clouds, cosmic rays, magnetic fields, and some other things that pass unnoticed by the naked eye filling the space between stars. This quite diverse and extended environment is known as the Interstellar Medium (ISM), which is coupled with a vast range of radiation from the whole electromagnetic spectrum that pervades the ISM and is known as the Interstellar Radiation Field (ISRF).

While at first, due to its dim nature, ISM can be thought to be less relevant than stars themselves, it has a crucial role in most of the physical and chemical processes that occur in the galactic environment, being the place where stars form and also where new matter and energy are released when stars end their lives via supernova explosions or as planetary nebulae. There is a very complex set of phenomena that characterize the ISM, from the atomic/molecular scale, passing through magnetic fields, to gravitational waves, which are inhomogeneously distributed all over the Galaxy, with dramatic changes of density and temperature from one place to another.

ISM does represent only around $\sim$ 0.5 % of our galaxy mass, mostly confined to the galactic disk, where it accounts for $\sim$ 10 - 15% of the disk's matter, with a peak towards the galactic plane and along spiral arms, despite being quite inhomogeneously spread at smaller scales. The densities in the ISM are really small in comparison to Earth, ranging from around 10^{-26} g cm^{-3} in the emptier spaces to 10^{-18} g cm^{-3} in the densest regions, which is more than a dozen orders of magnitude less particles per cubic centimeter than the outer part of the Earth atmosphere. In terms of chemistry, the ISM composition varies greatly from region to region, with some areas exhibiting chemical abundances similar to those found in the Sun and its surroundings, while others exhibit overabundances of certain species, as seen in molecular clouds. While metals, as astronomers dub any heavier than helium species, are

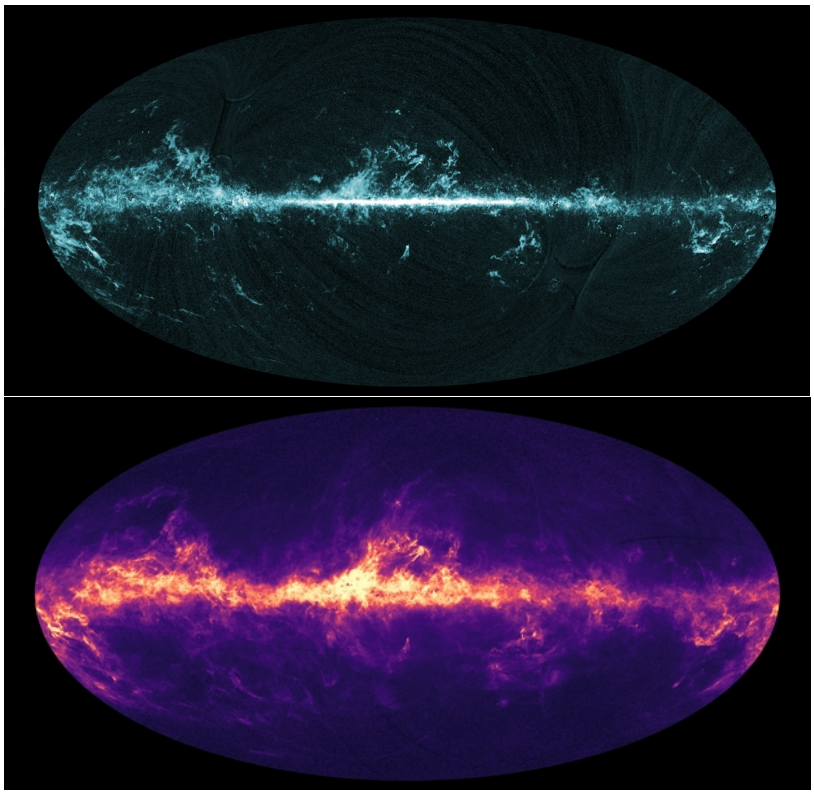

FIGURE 2.1. All sky views of carbon monoxide (CO) distribution, used to trace molecular clouds, as seen by Planck (Top, Credits to ESA/Planck Collaboration), and Milky Way interstellar dust, based on observations performed by ESA's Gaia satellite between July 2014 to May 2016 (Bottom, Copyright to ESA/Gaia/DPAC)

inhomogeneously distributed all over space, in cold-dense conditions they tend to *disappear* from the gas phases of the ISM, a phenomenon often named *depletion*. Overall, the most common metals C, O, and N, are depleted by a factor of $\sim 1.2 - 3$, but species heavier than them can be depleted by factors $\sim 10 - 100$. It is estimated that approximately 1% of the total interstellar mass is trapped in or forms part of interstellar dust grains.

2.1.1 Gas in the ISM

The main part of the interstellar medium itself consists of a gaseous medium composed of several chemical species. Among all those species, hydrogen is by far the most abundant one, making up to ∼70% of the total gas mass, followed by helium with a lower yet still considerable ∼28% of it, while the residual percentage is a mix of all the *metals* present in outer space.

In this gaseous medium, temperature and density are without doubt the most important structural parameters, and having a good description of them can give a good characterization of a specific zone under study.

How ISM gas is characterized is quite straight-forward, as it depends only on the chemical state of hydrogen, due to its extremely high abundance, coupled with the chemically inert nature of helium under standard conditions. Each *phase* of ISM gas depends on the hydrogen state, generally appearing in one of three different chemical forms. About 60% appears as neutral, atomic hydrogen (labelled as H or HI); another 23% appears in ionized forms (tagged either as H^+ or HII); and the remainder, approximately 17%, appears as molecular hydrogen, aka, H_2 (Draine, 2011).

Neutral Gas

The *neutral medium* is the phase where most of the ISM gas is present. It can be divided into two more specific layers: the *Cold Neutral Medium* (CNM), which corresponds to around 40% of atomic hydrogen, located in denser cold HI clouds with low temperatures (T $\sim$ 100 K), and the *Warm Neutral Medium* (WNM), which represents the other 60% distributed in the more diffuse and warmer inter-cloud medium with temperatures around T $\sim 10^4$ K. These two phases can be studied at optical and UV wavelengths and also traced with the atomic hydrogen 21-cm line.

Early investigations into the structure of the ISM focused on neutral atomic hydrogen, presuming it to be in thermal equilibrium. The so-called two-phase model (Field et al., 1969) was developed based on this assumption. This model provided two potential thermally stable ISM system solutions: one for dense, cold HI clouds and another for inter-cloud diffuse warmer gas, which we now refer to as CNM and WNM, respectively.

Over the years, with the improvement of available tools, this model has been expanded to include more distinct phases of ISM according to its properties, which we will review in the following sections.

Ionized Gas

While the neutral medium is the most easily studied of all ISM phases, it cannot cover the entire image of the ISM gas medium. There is a phase of ISM gas medium that is heated to very high temperatures ($\sim 10^5 - 10^7$ K) by supernova shocks and similar high-energy phenomena (Smith et al., 2013), especially at the edge of clouds, and dubbed as *Hot Ionized Medium* (HIM).

In terms of size, this is the largest phase of all, occupying roughly half of our galaxy volume (Tielens, 2005; Smith et al., 2013), despite accounting for a very small fraction of the total mass due to its extremely low density ($0.003 - 0.0065$ cm^{-3}). Because the gas in the HIM is collisionally ionized as a result of being subjected to shocks and high temperatures, it is possible to observe some highly ionized forms of some elements, such as O**VI** or N**V** (Draine, 2011), to name a few.

This particular phase was first mentioned/included by McKee and Ostriker (1977) on an expanded form of Field et al. (1969) two-phase ISM model, pointing out the existence of a third highly ionized phase that presented extremely similar temperature and chemical state conditions as those found in the sun's corona, so they named it *Coronal Gas*, the actual HIM.

However, HIM is not the only ionized phase of the ISM gas medium; there are also regions with very diffuse (~ 0.1 cm^{-3}) but warm (T $\sim$ 8000 K) gas, known as the *Warm Ionized Medium* (WIM). This phase does contain most of the ionized gas mass that is kept ionized by the energetic radiation of early type stars and, to a lesser degree, by white dwarfs and other stellar populations (Smith et al., 2013). The evidence for this gas phase originally came from optical and UV absorption line observations of ionized species against background sources, as dispersion of pulsar signals, and through the Hα recombination line emission (Tielens, 2005; Klessen and Glover, 2016).

The Molecular Gas

Although a great fraction of the neutral gas is in the form of cold atomic gas in the CNM, there is also some gas in the molecular state and it is typically studied separately from their atomic counterpart.

In galaxies where atomic gas predominates, as our Milky Way does, molecular gas tends to lie into discrete clouds, commonly known as Molecular Clouds (MCs), that are confined in a very thin layer in the Galactic disk (Lequeux, 2005; Klessen and Glover, 2016) and serve as the cradles for future stars. The size and mass of these clouds cover a vast range of values, but they all share a common property, they appear *visually dark* to us, having extinctions $A_V \gtrsim 3$ mag towards their *central* parts, making their observation viable mostly at infrared, sub-millimeter, and radio wavelengths/frequencies.

As the name MCs indicate, the density of these objects is dominated mainly by molecules, especially molecular hydrogen (H_2), followed-up relatively close by carbon monoxide (CO), that present a CO/H_2 ratio of $\sim 10^{-4}$ (Tielens, 2005). Inside these molecular clouds the star formation process takes place.

While H_2 is the most important species in molecular clouds, paradoxically, it was not observed in space for a long time, until the development of ultraviolet Astronomy in the early 70's, when CO molecule was found and measured, still used as a tracer of H_2 on our days, due of the difficulties in observing H_2 directly. This discovery was a great revolution in all terms, even when other molecules as CH and CN were already detected several decades before. In Savage et al. (1977) some measurements of H_2 column densities were provided which led to the very first estimates of space-averaged density and temperature of the molecular gas in Sun neighborhood.

It is important to note that all these *phases* definitions are just a method to simplify the way we study the ISM gas medium and do not represent an actual separation of them. With that in mind, we can define some phases more related to particular physical processes that happen during the life cycle of stars and the ISM's interaction with them, but they would not be as easily distinguishable as the ones described before. Good examples of this particular cases are HII regions, gas surrounding newly formed OB stars, that is continuously ionized by them and the high density outflows produced by evolved cool stars (Draine, 2011).

2.1.2 Dust

In denser regions of the ISM, surrounded by the interstellar gas, there exist also small solid parcticles, commonly labeled Dust Grains. Those grains are mostly composed by a combination of carbon, silicates and ices, but they can also be more complex molecules, as Polyciclyc Aromatic Hydrocarbons (PAHs).

They represent around $\sim 1\%$ of the total mass of the ISM and their existence does manifest through the reddening and extinction of background starlight, that gives rise to some *dark patches* in the night sky, and also through their interaction with the Galactic magnetic fields as can be measured from polarization effects.

The principal role of Interstellar dust grains is to act as a coolant for their surroundings, and to shield molecular gas from stellar radiation that would otherwise dissociate/ionise it.

Also, dust grain surfaces serve as the sites for molecules formation, especially H_2, as hydrogen atoms via physical and chemical absorption processes and trapped there, diffusing

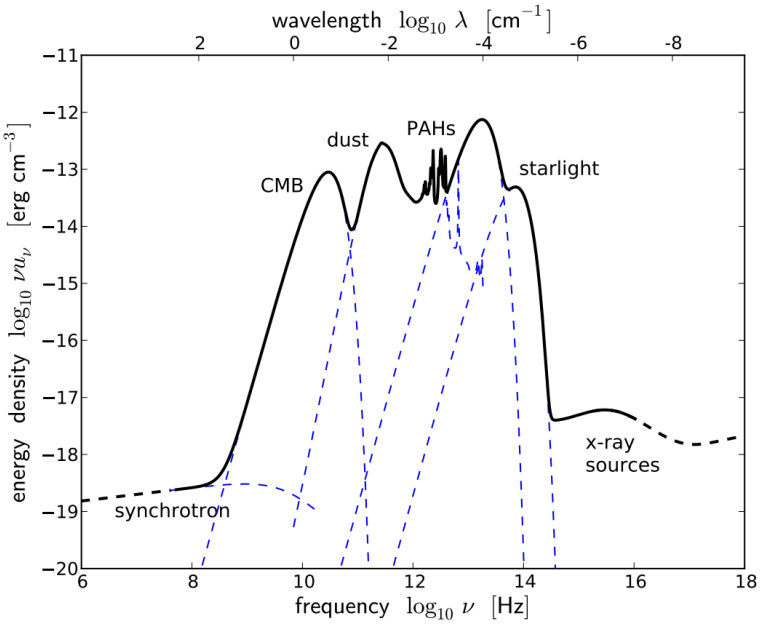

FIGURE 2.2. Schematic sketch of the energy density of the interstellar radiation field at different frequencies/wavelengths. Taken from Klessen and Glover (2016) and references therein.

through the surface until they interact with an other atom, forming an hydrogen molecule as a result, that will desorb back to the medium.

When studying the extinction curves produced by dust, there is something easily noticeable, and it is that silicates and graphite are the main constituents of dust, following a power-law size distribution

$$N(a)da \propto a^{-3.5}da$$

This relation is named the Mathis-Rumpl-Nordsieck (MRN) distribution, which is valid over a range of radii from about 0.005 μm to ~ 1 μm (Mathis et al., 1977). What can be concluded from this distribution is that most of the interstellar dust mass is located in the larger grains, but smaller grains dominate in terms of surface area (Tielens, 2005).

Dust grains are also often covered with water and carbon monoxide ice mantles. The grains composition is not fixed, being able to change according to the grain environmental conditions or through collisions with other grains, gas-grain reactions, cosmic rays, and more.

2.1.3 Additional components of the ISM

Radiation

While gas and dust are more noticeable as ISM components, alongside them, another important component of the ISM is radiation, spanning the whole electromagnetic spectrum, which is known as the Interstellar Radiation Field (ISRF). Radiation has multiples sources, coming both from the insides of our own galaxy but also from extragalactic sources. The interaction between gas, dust and this radiation field is what determines the chemical and thermal state that ISM gas will have.

In the case of chemistry and ionization, their state will be determined mostly on how photochemical processes affect the particles and molecules in a determined region, and on the radiation energy flux.

From a thermodynamic point of view, gas and dust present a quite different behavior, despite being tied to each other. In particular, gas is heavily influenced by energetic electrons released from atoms and dust grains, a process known as photoelectric heating, whereas dust is primarily influenced by the absorption and re-emission photons interacting with it.

The ISRF has different energy densities depending on the frequency or wavelength at which we measure it, which are depicted in Fig. 2.2. When frequencies are $\lesssim 1$ GHz, the primary source of radiation is synchrotron emission from relativistic electrons spiraling around the galactic magnetic field lines. At even lower energies, the Main Extragalactic source of radiation, that is the Cosmic Microwave Background (CMB), takes over as the most significant radiation source.

The infrared part of the energy spectrum is dominated by dust particles and Polycyclic Aromatic Hydrocarbons (PAHs), as they effectively absorb starlight with wavelengths shorter than their diameters, typically less than ~ 1 μm, (Draine, 2011), and then radiate this energy back into the ISM at longer wavelengths. Massive stars act as the primary radiation source at the highest frequencies, either directly through their stellar far ultraviolet (FUV) radiation or indirectly at the highest frequencies through the x-ray emission from the hot plasma created by their death as supernovae.

Magnetic Fields

It is known that ISM is strongly affected by Magnetic Fields, as proved by observations. The mean magnetic field in the diffuse medium is about 10 μG. Magnetic fields represent a very important source of energy and pressure in the interstellar environment, but their specific influence/relevance in cloud dynamics or the star formation process is something that is still under investigation.

Cosmic Rays

Along with all the aforementioned ISM components, there are also really high-energy (above 100 MeV, but covering a vast range of energies) particles with relativistic behavior known as Cosmic Rays (CRs). These *rays* consist, in most cases, of protons, but they could also be bare atomic nuclei, which are heavier than hydrogen atoms, or high-energy electrons.

In cold, dense regions, CRs have a fundamental role in regulating the chemistry because, unlike ultraviolet (UV) radiation, which suffers of a high attenuation under these conditions, they can efficiently penetrate inside them. Because CRs are the primary source of ionization in these regions, they are responsible for a variety of processes, including the formation of atomic hydrogen via the ionization (and sometimes dissociation) of H_2 molecules, as well as other significant changes in the dynamics of dense regions.

One particular effect of CRs over the dynamics in high density environments is the alteration they produce in the electron fraction, that directly regulates the degree of coupling of gas with the magnetic fields. This also alters the timescale for cloud collapse. CRs are also responsible for providing heating and energy to dust grains and are involved in several other processes.

2.1.4 ISM State

Although all previously mentioned phases of the ISM do co-exist in apparent pressure equilibrium with a median pressure of p $\sim$ 3500 K cm^{-3}, treating the ISM that way could be read as oversimplifying the topic (Smith et al. (2013).

The truth is that the ISM is very dynamic, being strongly dependent on the physics driven by massive stars. A proof of that is that while supernova explosions and stellar winds from massive stars expand through the diffuse medium in the form of fronts, they interact with cold molecular gas and convert it to hot HII. This hot gas from the HIM can cool to lower temperatures via radiative cooling, giving rise to the WIM, then the WNM, and finally, with small perturbations induced cooling, the CNM (McKee and Ostriker (1977).

Another thing is that the ISM is a medium with a high degree of turbulence. While we do not know the origin of interstellar turbulence yet, we cannot neglect how noticeable its effects are. As can be seen through the large-scale motions and shocks it produces, what would be otherwise distinct phases are being constantly mixed, which would lead to regimes that are far from pressure equilibrium.

In Facts, it is thought that a combination of compressive motions caused by turbulence and global instabilities can trigger the transition from warm, tenuous, mostly atomic gas to the dense, cold, fully molecular phase found in molecular clouds. Further perturbations can cause the complete collapse of these structures, giving rise to the formation of stars within them, as mentioned before (Smith et al. (2013).

2.2 Molecular Clouds

As was mentioned in Sec.2.1.1, molecular clouds are known to be the cradles of stars and star clusters (Lada and Lada, 2003), which makes the star formation process heavily dependent on the physical structure and the dynamical state of these gas complexes. This in turn depends on how these structures initially form, with a clear consensus on this topic still missing.

When observing molecular clouds at visible wavelengths, they appear as dark patches clashing with the bright stellar background. This dark appearance is caused by the dust grains around or within them, which absorb and scatter said background starlight. In order to look into them, infrared wavelengths should be used, or specific molecular lines employed, as was done in Dame et al. (2001), shown in the top panel of Fig. 2.3.

MCs come in a wide variety of sizes, but in general terms, they appear as filamentary and wind-blown structures. Due to their length scale and coherent velocity structure, it is estimated that this filamentary structure is an intrinsic trait of these clouds and not a consequence of external factors like star formation (Bergin and Tafalla, 2007).

Although these objects appear to have quite complex shapes, molecular clouds in general present a clumpy and hierarchical configuration, with subunits of smaller size appearing within large ones as seen in Fig. 2.3 top panel. They tend to organize fractally with a volume boundary dimension D of 2.3 $\pm$ 0.3; however, at smaller scales, this self-similarity breaks down (Bergin and Tafalla, 2007).

While most authors adopt the classification nomenclature proposed in Williams et al. (2000) for MC, the naming process of molecular complexes and substructures tends to be chaotic. Following Williams et al. (2000), these clouds are considered to be formed by gravitationally bound clumps that can form clusters or associations of stars, and at the same time,

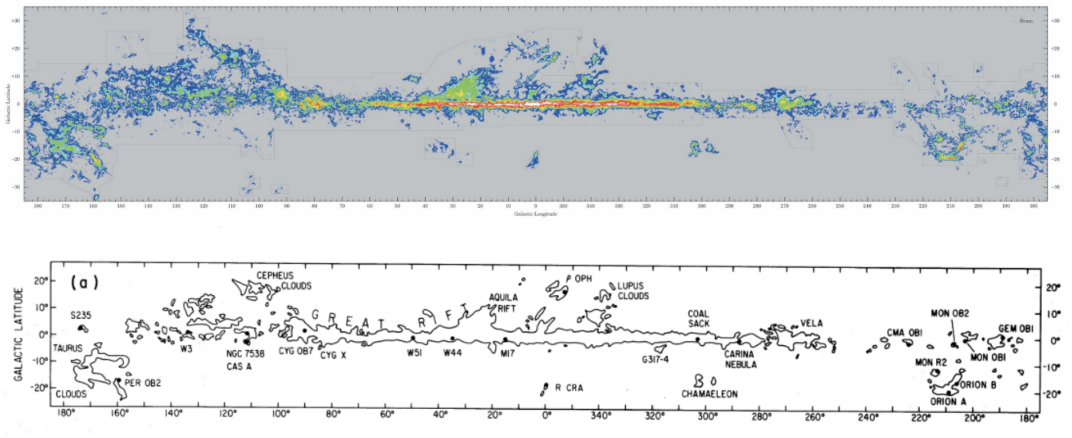

FIGURE 2.3. Top: The Milky Way in CO from the most recent complete survey of our Galaxy in CO (Dame et al., 2001). Bottom: Molecular clouds name in the Milky Way with CO contour, from Dame et al. (1987), Taken from Spilker (2021)

those clumps are composed of smaller cores from which single or multiple stars will be born later in their evolution.

What characterizes these clouds is the fact that they are really massive and large too, having masses that go from 10^3 to 10^4 $M_\odot$ and sizes of a few pc for the smaller Cold Dark Clouds (DCs), up to $10^4 - 10^7$ $M_\odot$ and from 20 to 50 pc, respectively, when referring to the more distant Giant Molecular Clouds (GMCs) (Murray, 2011).

In most cases, the properties of clumps within clouds seem to follow a power-law distribution. For example, the mass of clumps frequently exhibits a distribution of the form $dN/dM \sim M^{-\alpha}$, as does the mass of stars. However, for the clumps, the range in which α lies is quite narrow, between 1.4 and 1.8, unlike the steeper $\alpha = 2.35$ found by Salpeter (1955) for stars, implying that, for the clump distribution, most of the mass is contained in massive clumps, while the stellar distribution of mass is dominated by low-mass objects (Bergin and Tafalla, 2007). When we zoom in to smaller scales, we see that roughly 25% to 35% of the mass of the clumps is located along the filaments, in quasi-spherical objects known as cores, where density increases dramatically, exceeding 10^4 cm^{-3}. They are the location where the star-formation process occurs (Krumholz, 2015).

Molecular clouds are also characterized by a complex velocity structure, presenting thermal broadening on molecular lines with velocity differences of the order of 1 km s^{-1}. These clouds obey a linewidth-size relationship, with the velocity dispersion σ being dependent on the physical size L of the cloud as σ (km s^{-1}) = $1.1L(\mathrm{pc})^{\,0.38}$ (Larson, 1981; Krumholz, 2015). As MCs lack systematic motion patterns like rotation, expansion, or infall, to name a few, the origin of this velocity dispersion is suggested to come from turbulence, coupled with supersonic motions, and probably a magneto-hydrodynamical nature.

According to the ISM turbulence energy spectrum $E(k)$, which represents how energy is distributed at different spatial scales, the best way to describe turbulence in MCs is compressible and shock-dominated, which corresponds to Burgers-type turbulence with $E(k) \propto k^{-2}$ (Krumholz, 2015; Federrath, 2016). This means that at smaller scales, turbulence tends to dissipate, provoking denser, smaller structures to move at a slower rate than the surrounding large-scale, low-density material, showing a lot lower levels of turbulence and internal motions of subsonic order (Bergin and Tafalla, 2007; Krumholz, 2015).

Also, last but not least, molecular clouds are recognized to be highly magnetized. Frequently, the line-of-sight (LOS) magnitude of the magnetic field is calculated from Zeeman splitting observations, while its morphology can be estimated using dust grain polarization methods its morphology can be estimated (Bergin and Tafalla, 2007). In dark interstellar cloud conditions, the magnetic field is frozen to the gas, due to this, the ability of the magnetic field to counteract the action of self-gravity can be critical to their equilibrium balance. This issue had not been resolved yet, however, with some authors pointing out sources with magnetic field strengths on the verge of being critical and others finding sources slightly supercritical (Heiles and Crutcher, 2005; Crutcher, 2012).

Recent observations show that magnetic fields have a mostly constant maximum strength at ~ 10 μG when densities are less than nH ~ 300 cm^{-3}, increasing with density with a power-law exponent of $\kappa \sim 2/3$ (Crutcher, 2012). Following that logic, the magnetic field intensities in the densest regions should reach around ~ 100 mG. However, as there are a lot of uncertainties in the theory of maser polarization and the depletion of typical tracers, the reliability of these of these values at core levels is questionable (Crutcher, 2012).

2.2.1 Starless Cores

As mentioned before, as we go to lower scales on molecular clouds, we can find some compact structures, dubbed as *cores*. Those structures are mostly overdensities that are classified according to their evolutionary state. Among them, the ones that have not formed stars yet, known as starless cores, are the most important for this work.

They can be described as small, dense, self-gravitating clouds supported largely but not entirely by thermal pressure. Their densities are quite high (nH_2 $\sim 10^4$ to 10^6 cm^{-3}) with linear scales of tenths of pc and total masses of a few solar masses, and they are thought to be future rather than current star formation sites (Lee et al., 1999; Di Francesco et al., 2007; Bergin and Tafalla, 2007). Over time, some detailed observations of individual starless cores as Tafalla et al. (2004), have shown that these cores have densities that closely match those of pressure-confined hydrostatic spheres, known as Bonnor-Ebert or BE spheres (Bonnor, 1956), although the conditions of said spheres are not necessarily met in starless cores.

Despite most starless cores sharing a similar structure, it has been observed that they are far from being all the same. For example, observations of L1517B indicate presence of isothermal gas and show spectral line profiles indicative of little motion or possibly expansion (Tafalla et al., 2004; Sohn et al., 2007) while observations of L1544 indicate that temperature varies highly from center to edge (Crapsi et al., 2007) showing spectral line profiles consistent with an overall contraction Keto et al. (2004); Sohn et al. (2007). A similar contrast has been seen between the starless cores B68 and TMC-1, as CO observations of B68 show that toward the edge of the core the excitation temperature rises (Bergin et al., 2006), with spectral line profiles being consistent with internal oscillations (aka. sound waves) (Lada and Lada, 2003), while observations of CO isotopologues in TMC-1C (Schnee et al., 2007) indicate an excitation temperature decreasing toward the edges and that the cloud is contracting.

Some studies suggest that the starless cores can be separated in two distinct classes, thermally subcritical and thermally supercritical depending on whether their central densities are less or greater than a few 10^5 cm^{-3} respectively.

The reason behind this specific density value is that first, at this density, gas cooling by collisional coupling with dust is about as efficient as cooling by molecular line radiation, so

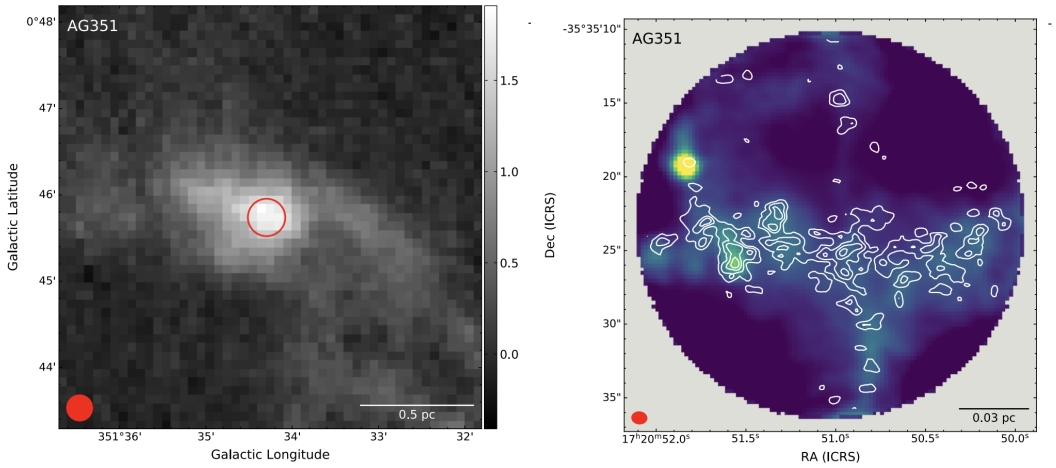

FIGURE 2.4. Maps of the continuum emission of clump AG351 at 870 μm seen with APEX by the ATLASGAL survey (left) and ALMA in band 7 with o-H_2D^+ contours overplotted (right). This clump has been discovered to contain several pre-stellar cores. Adapted from Redaelli et al. (2021)

the gas temperature in the center of the supercritical cores is therefore significantly lower than in their envelopes and lower than found anywhere in the subcritical cores; and second, at this density, the cores of a few $M_\odot$ are at critical dynamical stability with respect to gravitational collapse.

With that in mind, it is possible to deduce that thermally subcritical cores are stable against gravitational collapse and that their dynamics may be dominated by oscillations (Aguti et al., 2007). In contrast, the supercritical cores are unstable, with predominantly inward velocities (Sohn et al., 2007; Schnee et al., 2007).

2.2.2 Pre-Stellar Cores

The first step to describe the star formation process is the formation of cold dense cores of molecular gas and dust. When one of these cores does not contain a stellar object, it is referred as starless. Among those starless objects, the ones which are already gravitationally-bound, aka, present the initial conditions for protostellar collapse, are commonly named pre-stellar cores. The latter represent an important subset of starless cores, and present high central densities ($nH_2 > 10^5$ cm^{-3}) and low central temperatures ($T < 10$ K). In Fig. 2.4 we can see how a clump containing some pre-stellar cores looks at different wavelengths as seen in Redaelli et al. (2021).

Pre-stellar cores are sources on the verge of contraction that have not yet formed a protostar. Studying the physical structure and kinematics of pre-stellar cores is crucial to having a comprehensive view of the initial conditions for core collapse. The peak emission of these cold cores is in the submillimeter regime, so that is the best band to study them though that range can be expanded to far infrared with modern high-sensitivity multiband imaging. This is useful for the study of molecular spectra, which have been extensively used as diagnostics for dense cloud cores. Furthermore, hyperfine transitions have been shown to be effective probes of the physics and chemistry of molecular clouds (Sohn et al., 2007; Lique et al., 2015)

The precise mechanisms by which gravitational collapse occurs at sub-parsec scales remain unknown until the present days, though it is well understood that this collapse will

result in the formation of a pre-stellar core, which will eventually end transforming into one or more stars.

Turbulence has been recently reported to be one of the key ingredients for this process, creating overdensities to trigger core formation while also counteracting the effects of gravity in the denser regions of these objects (McKee and Ostriker, 2007). However, gravity and turbulence are not the only physical processes that are expected to be relevant for the collapse of these objects, as in the phenomenology of the star formation process, magnetic fields and dynamical chemistry networks are included too (Tassis et al., 2012; Girart et al., 2013, and references therein). It is not yet clear, however, which of all these mechanisms has dominance over the others.

Chapter 3

Chemistry in Cold Dense Regions

In the previous chapter, we introduced the ISM, the molecular clouds, and its substructures. Particularly, we introduced the properties of molecular gas in MCs, but we did not establish a clear way to differentiate them from diffuse atomic clouds.

The principal way to understand the transition between the atomic and the molecular medium is studying the chemical state of hydrogen and carbon, requiring the former to be in H_2 form while the latter in CO (Klessen and Glover, 2016).

If these species are found primarily in the aforementioned forms, we can discuss molecular clouds and their chemistry. More than 200 different molecules have been discovered inside molecular clouds, (Tielens, 2005), all potentially linked through extended networks of chemical reactions.

3.1 Gas-Phase Chemistry

When compared to Earth conditions (n $\sim 10^{19}$ cm^{-3}), interstellar clouds are cold ($T_{gas} \sim 10$ K) and have low densities (n $\sim 10^4$ cm^{-3}). These conditions allow only two-body collisions, which represent the main mechanism through which chemical reactions occur in the gas phase.

$$A + B \rightarrow C + D$$

These reactions occurs at a rate quantified by the rate coefficient k (cm^3 s^{-1}), which quantifies the abundance decrement of species A (n_A) and B (n_B) over time as it reacts between them.

$$\frac{dn_A}{dt} = \frac{dn_B}{dt} = -kn_A n_B, \tag{3.1}$$

while also measure the increase in abundance of species C (n_C) and D (n_D) as the reaction continues

$$\frac{dn_C}{dt} = \frac{dn_D}{dt} = kn_A n_B, \tag{3.2}$$

where n$_i$ (cm^{-3}) is called the number density of the i-th species.

Following that is possible to conclude that, as for some specific reaction k gets larger, then it will proceed faster, being more efficient than the ones where k is smaller, that will be slower paced. However, the number of available species n_i is also a major player in the efficiency of this process.

The value of k in most cases depends on temperature, and when the reactants are gas-phase species it is given by the following equation

$$k(T) = \mathcal{A}\left(\frac{T_{\rm gas}}{300K}\right)^{\beta} e^{-\gamma/T_{\rm gas}} \tag{3.3}$$

known as the modified Arrhenius equation. In this equation, β-coefficient represents the explicit dependence on temperature, while the γ-coefficient represents the activation energy for the reaction, that is a possible energy barrier required to trigger it.

For a more general case, the net rate of change in the abundance for any ith species involved in a reaction is given by the equation

$$\frac{dn_{\rm i}}{dt} = \sum_{i \in F_i} \left(k_i \prod_{\rm r \in R_i} n_r n_i \right) - \sum_{i \in D_i} \left(k_i \prod_{\rm r \in R_i} n_r n_i \right) \tag{3.4}$$

where the first summation represent the species formation and the one preceded by the minus symbol the destruction ones.

On interstellar clouds many kinds of gas-phase reactions can occur, with reactions between ions and neutral species representing the most efficient paths to form molecules. Among all the species that form thanks to this kind of reactions, CO is without doubt one of the most important, having its formation pathway the following steps:

$$\begin{aligned} \mathrm{C^+ + OH} &\rightarrow \mathrm{CO^+ + H} \\ \mathrm{CO^+ + H_2} &\rightarrow \mathrm{HCO^+ + H} \\ \mathrm{HCO^+ + e^-} &\rightarrow \mathrm{CO + H} \end{aligned} \tag{3.5}$$

that is crucial to the transition from cold, atomic gas to molecular regimes.

At the same time, some common tracers used for observational purposes do form from the reactions between neutral species and the most important ionic species for the chemistry of dense cores, the trihydrogen cation $\mathrm{H_3^+}$, such as $\mathrm{HCO^+}$ through

$$\mathrm{H_3^+ + CO} \rightarrow \mathrm{HCO^+ + H_2} \tag{3.6}$$

and $\mathrm{N_2H^+}$ through

$$\mathrm{H_3^+ + N_2} \rightarrow \mathrm{N_2H^+ + H_2} \tag{3.7}$$

Those ion-neutral reactions are considered the most efficient ones in gas-phase chemistry, as they are really fast, mostly due to their general independence from temperature and lack of activation barriers.

There is also another important type of reaction in gas-phase chemistry, among neutral species, as for example

$$\begin{aligned} \mathrm{O + OH} &\rightarrow \mathrm{O_2 + H} \\ \mathrm{H + CH} &\rightarrow \mathrm{C + H_2} \end{aligned}$$

In contrast to ion-neutral reactions, neutral-neutral reactions in general have activation barriers, that is $\gamma \neq 0$, and/or their α coefficients are quite small (from 10^{-10} to 10^{-12} $\mathrm{cm^3\ s^{-1}}$), making them relatively slow and inefficient. However, these reactions are quite important too, as they form part of several pathways for the formation of important species. The

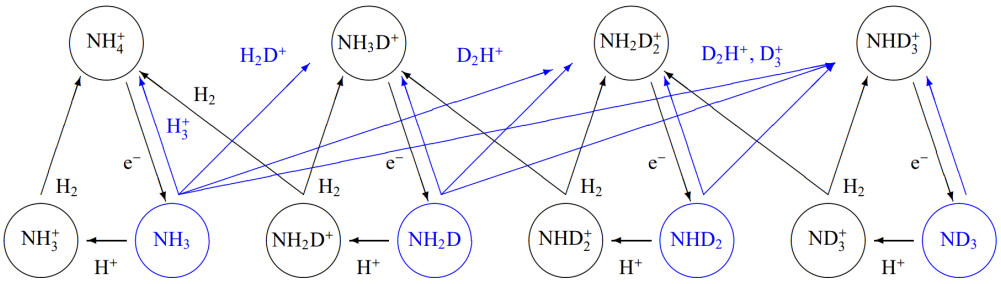

FIGURE 3.1. Principal reactions determining the abundances and spin ratios of deuterated ammonia isotopologues at late stages of chemical evolution in cold, dense cores. The blue arrows indicate the $NH_{3-X}\ D_X$ + $H_{3-Y}D_Y^+$ type of reactions. Taken from Sipilä et al. (2015)

formation of molecular nitrogen (N_2) from its atomic form (N) is the best example (Hily-Blant et al., 2010)

$$\begin{aligned} N + OH &\rightarrow NO + H \\ NO + N &\rightarrow N_2 + O, \end{aligned} \tag{3.8}$$

or the other formation mechanism for the production of CO via

$$CH + O \rightarrow CO + H \tag{3.9}$$

As in fact the reaction 3.8 is the main way N_2 is produced, its formation rate is ~ 10 times slower than that for C-bearing species (Suzuki et al., 1992), which affects general timescales of nitrogen chemistry, when compared with mainly gas-phase dominated oxygen and carbon chemistry.

When studying chemistry in dense cores, it is required to take into account cosmic rays, as they are the main (and only) available ionization source that can penetrate through the high levels of extinction in these embedded regions. In fact, the chain of reactions that leads to H_3^+ formation is triggered by cosmic ray-driven ionization, which occurs when a CR particle ionizes molecular hydrogen:

$$H_2 + \text{crp} \rightarrow H_2^+ + H + \text{crp} \tag{3.10}$$

followed by the fast ion-neutral reaction:

$$H_2^+ + H_2 \rightarrow H_3^+ + H \tag{3.11}$$

There are several other important species that form mainly through CR ionization, with ammonia (NH_3) being one of them, that starts its formation pathway from ionized helium through the channel (Pineau des Forets et al., 1990; Hily-Blant et al., 2010):

$$He + \text{crp} \rightarrow He^+ + e^-, \tag{3.12}$$

which is followed by the reactions

$$\begin{aligned} N_2 + He^+ &\rightarrow N^+ + N + He \\ N^+ + H_2 &\rightarrow NH^+ + H \\ NH^+ + 3H_2 &\rightarrow NH_4^+ + 3H \\ NH_4^+ + e^- &\rightarrow NH_3 + H, \end{aligned} \tag{3.13}$$

and also water through the reaction of oxygen and the H_3^+ cation that enables the chain:

$$\begin{aligned} H_3^+ + O &\rightarrow OH^+ + H_2 \\ OH^+ + 2H_2 &\rightarrow OH_3^+ + 2H \\ OH_3^+ + e^- &\rightarrow H_2O + H \end{aligned} \tag{3.14}$$

As these reactions depend on CR ionization, it is required to have the effective rate for this kind of reactions, which is not given by equation 3.2, but instead by

$$k_{CR} = \alpha\zeta_{CR}, \tag{3.15}$$

where ζ_{CR} is the cosmic ray ionization rate (CRIR), that has typical values of $\sim 1.3 \times 10^{-17}$ s^{-1} (Sipilä et al., 2010). However, this value is still highly uncertain, and it is expected to vary greatly depending on the environment (see Bovino et al. 2020).

There is another and final important type of gas-phase reaction, called dissociative recombination (DR), a process that happens when an molecular ion is destroyed by an electron. This type of reactions controls the ionization degree $\xi_{ion} \equiv ne^-/nH_2$ of star-forming cores, so they are essential for the dynamical state of these objects, because ξ_{ion} directly affects both ion-neutral chemistry, and the ambipolar diffusion timescale (see Redaelli et al. 2019, and references therein).

Although most DRs are between chemical species, is possible too that gas-phase species interact with charged grains, as grains also have the ability to dissociate ions. In dense regions, grains are negatively charged most of the time due to the reaction

$$GR^0 + e^- = GR^- + \text{photon} \tag{3.16}$$

where GR^0 denotes neutral grains. For this type of reaction, contrary to what happens with CRs ionization, the coefficient rate follows the definition given by 3.2 but there are times when a Coulomb factor, commonly known as *the J-factor*, is required to correct its value and take into account polarization due to differences in the electric charges between the reactants (Walmsley et al., 2004; Pagani et al., 2009) This correction factor depends on the temperature and the charge of the grain, with

$$J(\tau, -1) = \left(1 + \frac{1}{\tau}\right)\left(1 + \sqrt{\frac{2}{2+\tau}}\right), \tag{3.17}$$

when grains have negative charge, and

$$J(\tau, 0) = 1 + \sqrt{\frac{\pi}{2\tau}}, \tag{3.18}$$

when grains are in neutral state, with $\tau = a_{gr}k_BT/e^2$ being the reduced temperature (Draine

and Sutin, 1987), where e is the electron charge, $a_{\rm gr}$ the effective radius of the grain, and k_B the Boltzmann constant.

For densities around 10^4 to 10^5 cm^{-3}, DR reactions triggered by free electrons tend to dominate with respect to the interactions with grains. However, as density increases, the number density of grains also does, so the fractional abundance of free electrons goes down, making DR reactions with grains more relevant under the said conditions.

All previously mentioned types of reactions are the most important in the conditions of molecular clouds, but that does not mean they are the only ones in the ISM. Good examples are photoionization and photodissociation due to UV photons emitted by stars, that can directly ionize/dissociate certain species, but in MCs conditions does not work as dust grains tends to absorb those photons, re-emitting them at lower frequencies. The reaction rate for these reactions depends on the extinction as $k_{photo} = \alpha\, e^{-\gamma A_V}$, and become negligible in dense cores where $A_V \geq$ a few magnitudes, and γ is around $2 - 3$.

3.2 Gas-Grain Chemistry

As mentioned in Sec. 2.1.2, around 1% of the ISM mass is on solid dust grains, having typically core sizes of ~ 0.1 μm. These grains form in cool and dense environments, as for example, the atmospheres of red giant stars, being released into the ISM by radiation pressure, stellar winds, or material thrown off by Super Novae (SNe) explosions.

Though dust grains are solid objects, they are quite fragile, so it is expected that while being affected by interstellar shocks they can be easily destroyed, at a much faster rate than the replenishment capacity stellar ejecta have. This suggests that there is an unknown formation mechanism working directly on the ISM which is responsible for the observed abundance of grains (Bergin and Tafalla, 2007). Although the formation path of dust is not completely understood, something that is clear is that due to their extinction features, most of the dust is expected to be in the cold, dark clouds of the ISM.

It is not possible to describe the chemistry within molecular clouds in a comprehensive way without talking about dust grains as they effectively shield inner regions from UV radiation, give the guarantee of more complex molecules formation that would be ionized or dissociated otherwise, and affect the gas thermodynamics.

While dust grains have positive charges in diffuse clouds due to the effects of photoionization, when they are inside cores, their charge is mainly negative, which directly provides an effective source for DR reactions at high densities. Also, they can provide sites on their surface in which molecules that have been adsorbed can react, forming much more complex structures (Yamamoto, 2003).

As there are high grain densities and low temperatures in molecular clouds, elements that are heavier than helium, aka *metals*, and a major number of molecules tends to stick onto the grains surfaces when they collide or interact with them, what is commonly known as adsorption or *freeze-out*. This *loss* of gas-phase species as they get trapped onto grain surfaces is commonly called *depletion* (Bacmann et al., 2002; Yamamoto, 2003; Tafalla et al., 2006) which is measured through the depletion factor, defined for any i-species to be

$$f^i_{\rm dep} = \frac{n_i^{\rm exp}}{n_i^{\rm obs}}, \tag{3.19}$$

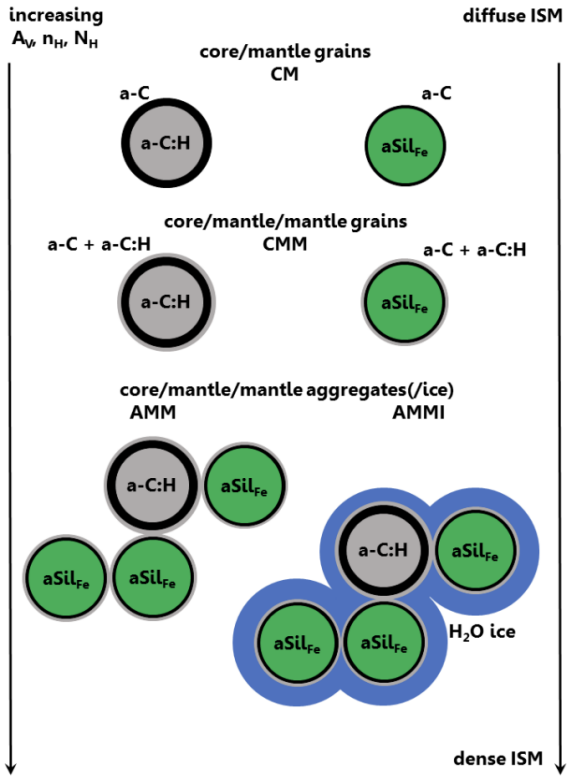

FIGURE 3.2. A schematic view of dust grains (layered) composition and stratification when going from diffuse to dense regions in the ISM. Taken from Ysard et al. (2016). Density, column density and extinction increases from top downwards.

where $n_i^{\rm exp}$ is the *expected* abundance of the i-species as if it did not went through depletion, and $n_i^{\rm obs}$ the real observed value.

The aforementioned ratio is most used by observational investigators, defined in terms of the observed column density of the i-species compared to the H_2 column density N[H_2], $X_i^{\rm obs}$, and that of the canonical one for the i-species $X_i^{\rm exp}$. For example, in the particular case of CO the depletion factor would become:

$$f_{\rm dep}^{CO} = \frac{X_{CO}^{\rm exp}}{X_{CO}^{\rm obs}}, \tag{3.20}$$

with $X_{CO}^{\rm exp}$ obtained most of times following a series of isotopic ratios and abundances at a certain Galactocentric distance (see Fontani et al. 2006; Giannetti et al. 2014), typically assuming to be equal to its canonical relative abundance of 1.2×10^{-4} in molecular clouds.

The structure of dust grains changes as more species continue freezing-out on their surfaces, getting somewhat fluffy while obtaining new layers or *mantles*, composed by H_2O, CO, and other similar molecules (See Fig. 3.2 and Allamandola et al. 1999; Bergin and Tafalla 2007). The adsorption rate coefficient for a given i-species in s^{-1} is

$$k_i^{\rm ads} = n_{\rm gr}\pi a_{gr}^2 v_i S = n_{\rm gr}\sigma v_i S, \tag{3.21}$$

where $\sigma = \pi\, a_{gr}^2$ is the cross-section of the grain, $v_i = \sqrt{8k_{\rm B}T_{\rm gas}/\pi m_i}$ is the thermal velocity in the gas of the i-species, $n_{\rm gr}$ the number density of grains, and S is the temperature dependent sticking coefficient, that is, the probability for the species to stay bound to the grain after a

collision, assumed to be unity for all species from here on.

As long as absorbed species stay on the surface of grains is possible for them to react with other species also trapped there, or they can be returned to the gas-phase via any desorption mechanism. The most common desorption mechanism is thermal desorption, given by Hasegawa and Herbst (1993)

$$k_i^{\mathrm{des,th}} = v_i e^{-E_{b,i}/T_{\mathrm{dust}}} = \sqrt{\frac{2n_s k_{\mathrm{B}} E_{b,i}}{\pi^2 m_i}} e^{-E_{b,i}/T_{\mathrm{dust}}}, \tag{3.22}$$

where v_i is the harmonic oscillator frequency for the i-species, n_s the number of sites for adsorption on the grain, T_{dust} the temperature of the dust grains, and $E_{b,i}$ is the binding energy in K of the i-species. However, this mechanism is not even effective in dense cores conditions, especially due to the low temperatures and long time scales for the process to happen, so in order to recover gas-phase species non-thermal processes are required.

Among the non-thermal desorption mechanisms in dense regions, the most common is caused by CRs induced heating of grains. When a dust grain is impacted by a CR particle, it gets transitionally heated up to $T_{\mathrm{dust}} \sim 70$ K, which allows the diverse species to desorb from the grain surface (Hasegawa and Herbst, 1993) at a rate given by

$$k_i^{\mathrm{des,CR}} = f(70\mathrm{K}) k_i^{\mathrm{des,th}}(70\mathrm{K}), \tag{3.23}$$

where the efficiency factor $f(70\mathrm{K}) = 3.16 \times 10^{-19}$ for a CRIR of $\zeta_{\mathrm{CR}} \sim 1.3 \times 10^{-17}$ s^{-1} (Hasegawa and Herbst, 1993). It is important to note that some explorations have been done around exothermic reactions on grain surfaces, showing that they can provide the required energy to desorb the formed molecules, this process called *chemical desorption*. Due to high uncertainties affecting this process, we will not further consider it on this work.

3.2.1 Formation of molecular hydrogen in the ISM

The formation of molecular hydrogen is one of the most important chemical processes in molecular clouds. The simplest way to form H_2 in the gas-phase is through

$$\mathrm{H} + \mathrm{H} \rightarrow \mathrm{H_2} + \gamma \tag{3.24}$$

However, this reaction has a very low rate coefficient, which means this reaction proceeds too slowly to be relevant in most cases. When settled under metal-free or low-metallicity conditions, H_2 has typical formation paths as: (Krumholz, 2015; Yoshida, 2019)

$$\mathrm{H} + \mathrm{e^-} \rightarrow \mathrm{H^-} + \gamma \tag{3.25}$$

$$\mathrm{H^-} + \mathrm{H} \rightarrow \mathrm{H_2} + \mathrm{e^-} \tag{3.26}$$

and (Klessen and Glover, 2016)

$$\mathrm{H} + \mathrm{H^+} \rightarrow \mathrm{H_2^+} + \gamma \tag{3.27}$$

$$\mathrm{H_2^+} + \mathrm{H} \rightarrow \mathrm{H_2} + \mathrm{H^+} \tag{3.28}$$

but not much theory development was required in order to recognize that these pathways are also highly inefficient to produce H_2.

In the present times, it is widely accepted that H_2 in the local Universe is mainly formed through grain catalysis. In the moment two hydrogen atoms end up adsorbed by a dust grain, they rapidly diffuse through the grain surface, reacting to form an H_2 molecule, which is quickly desorbed back into the gas-phase of ISM (Krumholz, 2015; Klessen and Glover, 2016).

We can re-write the adsorption rate for a i-species in s^{-1} given by Eq. 3.21 as

$$k_i^{\text{ads}} = \left(\frac{n_{\text{gr}}}{n_{\text{H}}}\right) v_i \sigma S n_{\text{H}} = x_{\text{gr}} v_i \sigma S n_{\text{H}} \tag{3.29}$$

with n_H being the number density of H nuclei. Hence, $x_{gr} = n_{gr}/n_H$ is called the fractional abundance of dust grains compared to H nuclei. For typical core values, say, with $x_{gr} \sim 10^{-12}$ and $a_{gr} \sim 0.1$ μm (Yamamoto, 2003) we obtain

$$k^{\text{ads}} \sim 5 \times 10^{-18} n_{\text{H}}. \tag{3.30}$$

As the adsorption timescale main dependence is the medium density, we can estimate it, in years, by

$$t^{\text{ads}} \sim \frac{3 \times 10^9}{n_{\text{H}}} \text{ years} \tag{3.31}$$

Dense cores have typical average densities of $n_H \sim 10^5$ cm^{-3}, that gives us $t^{ads} \sim 3 \times 10^4$ years, therefore expecting that adsorption occurs within a typical core lifetime.

On the other hand, as the CR desorption coefficient rate is already in s^{-1}, is easy to imagine that the desorption timescale is just the inverse of said value. It depends on the specific species, and to give some example, we have for H and CO that

$$t_{\text{H}}^{\text{des,CR}} \sim 500 \text{ years}, \quad t_{\text{CO}}^{\text{des,CR}} \sim 6 \times 10^6 \text{ years}. \tag{3.32}$$

From those values, we can extract that volatile species, as H is, can quickly return to the gas-phase while heavier species like CO, have higher binding energies, and can remain completely frozen-out on the surfaces of the grains during the core whole lifetime after being adsorbed by it (Yamamoto, 2003; Bergin and Tafalla, 2007), unless efficient non-thermal desorption is in place.

3.3 Deuterium fractionation

Hydrogren is by far the most abundant chemical species in the whole known universe. When is in its atomic form, it is formed by a single proton and a electron that orbits it, that is how commonly we find it, but as any other chemical species, we can find in other distinct forms depending on the number of particles that an hydrogen atom have on its nucleus.

Those hydrogen atoms with more than one particle on their nucleus are known as hydrogen isotopes. Though there are several forms, due to its abundance, there are two major ones: deuterium, also known as heavy hydrogen, with one proton and one neutron on its nucleus, and the uncommon tritium, which has three particles on its nucleus: one proton and two neutrons.

Deuterium and Tritium abundances compared to regular hydrogen are really low, with Tritium being almost negligible when compared with its *brothers*, while also being an unstable species that could only live for a few years. Due to these, tritium is not being considered

for this work, while on the other hand, deuterium has some special properties in ISM chemistry, so it requires further development.

Deuterium, as hydrogen, was formed during primordial nucleosynthesis in the first minutes after the Big Bang, with a cosmic fractional abundance of $\simeq 1.5 \times 10^{-5}$ that is still observable today (Linksy, 2003).

When observed in molecular cores, deuterium appears to be almost completely locked into the HD molecule (half-deuterated hydrogen molecule), with a fractional abundance consistent with the cosmic value with respect to regular molecular hydrogen. If enough low temperatures are reached, deuterium (D) in atomic form can finally be treated as a separate species as a result of the large zero-point vibrational energy differences with its main isotopologue, atomic hydrogen (H).

Deuterium fractionation (D_{frac} or *deuteration* Bacmann et al. 2003) is the phenomenon that consists in the abundance enchancement of deuterated molecules above the typical cosmic ratio, that is tied to the high depletion degree in dense molecular cores. Deuteration is the process of replacing a hydrogen atom in a molecule with a deuterium atom. A ratio between deuterated and non-deuterated species, such as N_2H+, is easily calculated.

$$D_{\text{frac}}^{N_2H^+} = \frac{N[N_2D^+]}{N[N_2H^+]} \tag{3.33}$$

which can tell us about the chemical state of an observed region. Deuteration in the gas phase begins with an ion-neutral reaction between HD and H_3^+, which is followed by continuous deuteration as

$$H_3^+ + HD \leftrightharpoons H_2D^+ + H_2 + \Delta E, \tag{3.34}$$

$$H_2D^+ + HD \leftrightharpoons D_2H^+ + H_2 + \Delta E, \tag{3.35}$$

$$D_2H^+ + HD \leftrightharpoons D_3^+ + H_2 + \Delta E, \tag{3.36}$$

where ΔE is a difference of energy, explicitly indicating if the nature of the forward (or reverse) reactions is endothermic or exothermic respectively. In the most common conditions, when H_3^+ and H_2D^+ react with CO molecules, they are efficiently destroyed as

$$H_3^+ + CO \leftrightharpoons HCO^+ + H_2, \tag{3.37}$$

$$H_2D^+ + CO \leftrightharpoons DCO^+ + H_2, \tag{3.38}$$

However, these last two reactions do not occur in cool environments with high depletion, as dense cores are by definition, due to the almost complete freeze-out of CO on the surface of dust grains, favoring deuteration reactions instead. In any case, the behavior of deuteration depends on many factors.

Deuteration and the gas temperature (T_{gas})

As previously demonstrated, reaction 3.34 is the starting point of deuteration chemistry and can occur both forward and backward.

In spite of this, as the backward reaction was explicitly labeled as an endothermic reaction, if put under typical conditions of cold molecular cores, it becomes almost incapable of happening, so it ends up being irrelevant in that regime. If temperatures rise to a higher

regime, it is possible that the activation barrier is overcome, allowing the backward reaction to compete with the forward one, lowering the net formation of the H_2D^+ ion.

Therefore, as high temperatures tend to stabilize the formation and destruction of deuterium-bearing molecules, having low temperatures is definitely a requirement in order to enhance the deuteration process.

Deuteration and Cosmic Ray Ionzation Rate (ζ_{CR})

As mentioned in Section 3.1, the formation of the main building block of deuteration, H_3^+, is initiated by a CR-driven reaction, so it is heavily dependent on it. Higher values of ζ_{CR} should therefore increase the formation of H_3^+ and, as a result, the deuteration process.

However, it is important to keep in mind that higher CRIR values should also enhance the desorption of CO from the surface of dust grains, bringing it back to the gas phase and causing an efficient destruction of deuterated molecules, counterbalancing the former process. In general, CO desorption is less efficient than increasing deuteration by increasing H_3^+ production and takes longer timescales.

Deuteration and depletion of neutrals

H_3^+ and H_2^+ are ions that readily react with abundant species to produce some others. As demonstrated in reactions 3.37 and 3.38 any interaction between them and CO could destroy the molecules responsible for deuteration; thus, if the gas-phase contains high levels of depletion for species such as CO, said reaction will not occur, enhancing the process of deuteration.

This statement can be extended to other neutral species with the ability to destroy, albeit on a much smaller scale, such as H_3^+ and H_2^+, as well as N_2. It is worth noting that taking this into account indirectly makes deuteration a density-dependent process, because higher densities imply higher depletion levels and thus higher deuterium fractionation.

Deuteration and spin-state chemistry

Last but not least, the most important factor on which deuteration depends is spin-state chemistry, a critical topic for fully understanding the chemistry in cold, dense regions. In principle, any chemical species composed of multiple protons, or deuterons, can exist in different spin configurations. In the particular case of molecular hydrogen, it contains two atoms, each of which is spinning in one of two possible alignments. This gives rise to two possible states, often called spin-isomers: the ortho-form, where both spins are parallel, and the para-form, where spins are aligned in an anti-parallel fashion. This distinction is most often made in a simple way, by adding an o (for ortho configurations) or p (for para configurations) as a prefix to the chemical formula of a specified molecule. In the case of molecular hydrogen, for example, the ortho and para forms can be written as oH_2 and pH_2, respectively.

It is important to note that there could be as many spin isomers as there are atoms or deuterons in a molecule. For example, the meta isomer appears when a molecule is formed by three atoms or deuterons and two of them have their spins aligned in a parallel fashion while the other is in an anti-parallel fashion, However, as we will not allow molecules with more than three atoms in our chemical network (see Sec. 4.3.1), we do not consider higher-numbered spin isomers than the already mentioned ones.

This is important for dense region chemistry because there is an energy difference of $\sim$ 170 K between each ground-state of these forms. Although these energies could seem non-relevant in environments with low temperatures, they can be quite *game changing*, as the backward form of reaction 3.34 does increase its efficiency with an enhanced abundance of oH_2 and oH_2D^+, thus becoming able to effectively compete against the forward form.

The relative abundance between the different spin isomers is labeled as the ortho-to-para ratio (OPR), and higher initial values of the OPR(H_2) will hinder the formation of deuterated molecules. Although the H_2 OPR has been observed to decrease over time, its initial value is currently unknown (see Troscompt et al. 2009; Vaytet et al. 2014; Lupi et al. 2021).

Over the past twenty to thirty years, studying deuterated molecules in star-forming regions has increased in popularity, being used as, for example, unambiguous tracers of the chemistry and kinematics of the densest and coldest gas reservoirs that escape from the mainly used molecules to trace (Caselli et al., 2002a, 2003; Pillai et al., 2012), or probes of the ionization fraction $x_{e^-} = n_{e^-}/n_{H_2}$ (Caselli et al., 2002b; Redaelli et al., 2019) and the cosmic-ray ionization rate (Shingledecker et al., 2016; Bovino et al., 2020). It is also suggested that deuteration can act as a chemical clock (Fontani et al., 2011; Brünken et al., 2014).

Also, it is important to note that deuteration is very sensitive to changes in the chemical and physical conditions of its environment. It has been observed to increase with time during collapse, while decreasing when a protostar forms as a result of deuterium main destroyer evaporation (Caselli et al., 2008; Fontani et al., 2015; Kong et al., 2015; Giannetti et al., 2019). However, which of the possible factors in play are causing this trend and, with it, the physical state of the core, are unresolved topics yet, being the aim of current debates on deuteration's usability for those purposes (Körtgen et al., 2019; Bovino et al., 2019).

Chapter 4

Methodology

In this chapter, we describe the resources we used to develop our project and what it consists of, first giving a brief description of the tools we made use of, then the setup of our simulations, to later talk about the results we obtained in Chapter 5.

4.1 The KROME Package

Our main goal in this work is to unveil the behavior of ammonia chemistry as it evolves on a simulated pre-stellar core, which makes us require tools that can solve chemistry coupled with magnetohydrodynamics (MHD) simulations. For this purpose, we had employed the KROME package Grassi et al. (2014).

KROME is an open source GNU-licensed chemistry package, in the form of library-like code, that, given a chemical network written in plain text format that contains the list of reactions with each reactant, product, temperature limit, and rate coefficients, will automatically generate the routines to solve the kinetics of the system. It includes both gas-phase and grain microphysics, modeled as a system of coupled Ordinary Differential Equations, constructed according to the rate equation method. Thus, it calculates the rate of change in the abundances of any given chemical species as defined in 3.4. It also provides several other options, such as many thermal processes, and can be easily coupled with radiative transfer schemes to consistently follow photochemistry and other similar processes that make this package a very flexible tool.

For this work, the KROME package will be used to follow the evolution of ammonia, its spin isomers and deuterated forms chemistry evolution over the 3D-MHD simulation results of M1 core from Bovino et al. (2019) using the chemical post-processing scheme developed by Ferrada-Chamorro et al. (2021).

4.2 Chemical Post-Processing

4.2.1 Context

Though astronomy is a very old science, dating back to the dawn of civilization, the link between it and chemistry was not established until the discovery of the first molecules in the ISM less than a century ago (Swings and Rosenfeld, 1937; Douglas and Herzberg, 1941).

Since that time, the study of chemistry in astronomical contexts has grown in importance over time. In present times, astrochemistry is considered a crucial part of any well-developed investigation, where the analysis of the chemical structure and evolution of any given system under study is required to have a comprehensive understanding.

However, including self-consistent chemical evolution in theoretical models is quite challenging, as, under the conditions of astronomical environments, there are several constraints that must be settled to keep the modeling consistent with even an oversimplified reality.

Directly comparing the timescales on which chemical reactions happen with other dynamical processes, they are very short, and the dependence they have on local properties of the medium, specifically density and temperature, is very strong.

If the goal is to do an accurate review of the evolution of any system as a whole, it would be a requirement to use on-the-fly (OTF) non-equilibrium chemistry calculations over the hydrodynamic evolution. This is especially true at galatic scales, where the system thermodynamics are affected by the state of the gas (Richings et al. 2014; Bovino et al. 2016).

When doing chemistry at galactic scale, most of the studies rely on chemical post-processing of the simulations performed. This process is done making use of pre-computed CLOUDY tables (Ferland et al., 1998, as in Pallottini et al., 2017; Pallottini et al., 2019; Arata et al., 2020) or determined from chemical networks assuming that photo-ionization occurs in equilibrium (Keating et al., 2020). However, efforts to incorporate non-equilibrium chemistry into simulations have increased, particularly in the last decade. These efforts have gone from simple primordial species (Gnedin et al., 2009; Katz et al., 2017; Pallottini et al., 2017; Lupi et al., 2018, to cite some) to more structured ones that included *metal* species (Glover et al., 2010; Richings and Schaye, 2016; Lupi and Bovino, 2020; Lupi et al., 2020).

Contrary to what happens at galactic scales, the complexity of chemistry increases heavily when simulations are done on small scales, such as those of pre-stellar cores or protoplanetary disks. The conditions during the star formation process, when pre-stellar cores form, are very high densities ($n_{H_2} > 10^4$ cm^{-3}) and also very low temperatures ($T < 20$ K), with a well-defined chemical structure determined by some chains of reactions (as mentioned in Chapter 3), that are characteristic of these environments (Caselli and Ceccarelli, 2012; Öberg and Bergin, 2021).

As previously stated, these conditions are ideal for heavy species freeze-out, which means that a large number of interactions between gas and dust reactions begin to occur on the surfaces of dust grains, increasing the complexity of the already complex structure of these objects (van Dishoeck, 2018). This causes chemical networks to also grow exponentially, making OTF calculations in the already expensive 3D magnetohydrodynamic (3D-MHD) simulations computationally very expensive. There is a need to include gas-grain interactions and grain surface chemistry when studying star-forming regions in order to gain a complete understanding of the chemical complexity and specific features observed in the aforementioned conditions.

Because most chemical model schemes are not robust and consistent enough, some relevant, unresolved features have been under scientific scrutiny over the last decades, such as the reason for high NH_3 abundances observed in the central regions of pre-stellar cores (Tafalla et al., 2004; Crapsi et al., 2007); or the convoluted processes governing the formation and evolution of interstellar complex organic molecules (iCOMs) (Jiménez-Serra et al., 2016; Punanova et al., 2018)

The common approach to studying these two cases is to build low-dimensionality models to address some questions in a more qualitative way, relying on a large parameter space to make them more reliable. There had been no consistent major works following the evolution of NH_3 chemistry in 3D simulations. .

Chemical post-processing, as its name suggests, involves running all the chemistry routines over the outputs of a simulation that has already been done in order to reduce the time and computational resources required. This method is based on selecting a sub-sample of resolution elements (aka. particles) from the results of MHD simulations without OTF chemistry and integrating chemical equations on the dynamical history of said elements.

This method presents some limitations; for example, it is most often applied to isothermal cases because doing temperature-dependent simulations requires an analytical solution of the thermodynamics or a minimal chemical network to follow the most relevant coolants. Also, the results depend on the number of particles considered for post-processing and the post-processing method used, which can lead to a critical accuracy loss.

Having those limitations in mind and to avoid accuracy problems, we made use of Ferrada-Chamorro et al. (2021) post-processing routine for this work, which assures us that our results would be good in terms of accuracy compared to OTF chemistry under similar conditions if we used at least one percent of the particles from the input simulation.

4.2.2 The Method

We made use of Ferrada-Chamorro et al. (2021) post-processing scheme in order to study the chemical evolution of NH_3 and its isotopologues. The authors conducted a comprehensive parameter study on it in order to obtain a complete validation of the technique used. Their post-processing method assumes that chemistry does not significantly affect the dynamical evolution of the system. That is true if the system is considered to be isothermal, as they assumed it to be, while relaxing this condition would necessarily require on-the-fly chemistry with at least a minimal network to track the thermal evolution of the gas Grassi et al. (2017), or at least an analytical solution for it.

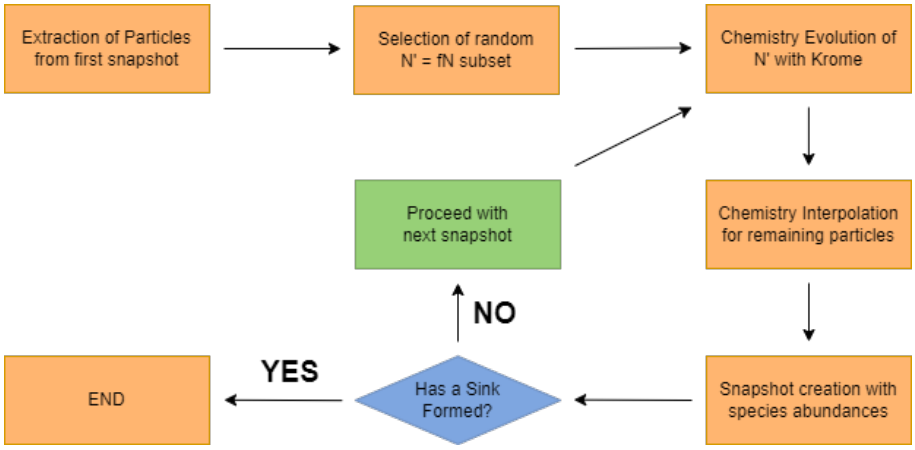

FIGURE 4.1. Schematic descriptive flowchart of the presented post-processing method, reproduction Ferrada-Chamorro et al. (2021) Fig. 1.

Starting from a standard hydrodynamic simulation of our system, say, without chemistry, they collected the outputs in which the history of its dynamical properties is stored, named snapshots. Over these snapshots, they applied the non-equilibrium chemical evolution, using the procedure resumed on 4.1 as follows

1. The density of each particle in the run is extracted from the simulation outputs, constructing a density evolution history and tracking particle IDs across multiple snapshots.

2. A subset $N' = f_{\rm part}N$ of the total N particles is selected in the simulation initial conditions (when $t = 0$), with $f_{\rm part} \leq 1$ being an user-defined parameter.

   As long as sampling the whole dynamic range of the simulation is required, no matter how much of the total number of particles is used to map the pre-stellar core and the background,

   They also enforced a user-defined number fraction $\xi_{\rm core}$ to be extracted from the particles sampling the core and the remaining ones from the low-density background surrounding it.

3. When the particles fraction are selected, the species abundances are initialised.

4. The chemical abundances of the N' subset of particles are then evolved using KROME, with a coarse integration time-step of of $\Delta T = {\rm m}\Delta t_0$, where Δt_0 is the time separation between snapshots and ${\rm m} \geq 1$.

   Over each integration step, the density of the particle is kept constant at the value obtained from the evolution history of every particle in the simulation at the beginning of each time step.

5. The species abundances for the remaining particles in the simulation (1 - $f_{\rm part}$) are derived from the closest post-processed particle in density-position space.

   In more detail, they binned the post-processed particle sub-sample as a function of density. Then, iterating over all non-evolved particles, the corresponding density bin for each of those particles is found, identifying the spatially closest evolved particle in the bin and associating its species abundances with the target particle.

6. After each step, a new snapshot of the simulation that includes the newly calculated species abundances is created. Then, the process is repeated from step 4, using the resulting abundances as initial values for the new step.

   This procedure continues to be applied until a sink particle is identified to avoid any artificial effect on the chemistry caused by the removal of the density due to the sink particle. In general, the post-processing can continue if the hydrodynamical simulations include a proper treatment of the protostellar feedback.

The authors made some considerations during their work. One of them is that $\xi_{\rm core}$ should be in principle tuned to the actual number of particles employed to map the core and the background in the simulation, respectively, noting that neglecting it, that is, assuming an homogeneous sampling of the entire particle distribution, would result in an oversampling of the background, which will affect the interpolation scheme.

When doing the interpolation, they considered it important to notice that, because of the intrinsic scatter in the particle density distribution resulting from the hydrodynamic evolution, the interpolation can be moderately affected by the particles chosen for the chemical evolution. In addition, the accuracy of the results will depend on the chosen interpolation scheme. Last but not least, all the calculation processes could be performed even after sink particles had formed, considering the proper caveats for that particular case.

This scheme was validated using it over the slow-collapse core M1 model from Bovino et al. (2019). First, they reviewed the effects of $f_{\rm part}$ doing three different runs for 0.1, 1, and 10% fraction of particles respectively, where the ones with smaller samples showed some incomplete or artificial features, especially for gas-grain dependent species, while, even with

1% of the particles used for the post-processing, gas-phase reactions dependent ones are well reproduced. They concluded that the general error on the calculations is always below 10%, and that $f_{\rm part}$ does not affect directly the abundances obtained, but choosing a low value for it will amplify the errors due to poor sampling.

Similarly, with the integration time, Δt, it was discovered that different time-steps affect higher density regions more directly while leaving lower density regions almost untouched, necessitating careful time step selection to keep the results in good agreement with the reference simulation. They also did some core-to-background particle ratios exploration, but both qualitatively and quantitatively the differences were completely negligible.

This post-processing routine was run with a FORTRAN90 code, in the density extraction for a subset of particles to be evolved, the chemistry calculations on them and the interpolation for the non-evolved particles coupled with a Python driver, for the selection, evaluation and creation of new chemistry-evolved snapshots.

4.3 Setup

4.3.1 Chemical network

In order to run the post-processing scheme, we need a well-defined chemical network for KROME to read and calculate species abundances. For this investigation, we have expanded the network used in Bovino et al. (2019); Bovino et al. (2020) and Ferrada-Chamorro et al. (2021) to include the formation and destruction of NH_3 and the hydronium ion (H_3O^+), along with their deuterated counterparts, to have a complete picture of NH_3 depletion. The following changes have been made to those networks:

1. We had included reactions of NH_3 and NH_3^+ with other species, but we kept the restriction of not allowing molecules with more than 3 atoms on the network.

2. For completeness, as suggested by Kong et al. (2015), we also incorporated the gas-phase formation of H_3O^+, keeping the restriction mentioned in previous step

3. Due to its relevance on the gas-phase formation of NH_3, a few reactions that included the NH_4^+ ion, following the schematic shown in Fig. 2 of Sipilä et al. (2015) were also added to the network (see Fig. 3.1).

4. As following consistently the evolution of these additional species was required, time-dependent adsorption and desorption reactions were incorporated for the following species: C, O_2, NH, OH, NH_2, H_2O, and NH_3, on top of those already mentioned in Bovino et al. (2019), under the same assumptions for these mechanisms.

Having all these considerations, the final chemical network includes 210 species and 8535 reactions in total. The initialization of the chemical conditions of the studied core was done assuming a fully molecular state, with the initial abundances being specified more in detail in Table 4.1. Also, the binding energies for all molecules that are affected by freeze-out reactions are taken from Wakelam et al. (2017), as summarised on Table 4.2.

TABLE 4.1. Fiducial initial abundances of the species in our network relative to the atomic hydrogen abundance n_{H} (i.e., n_i/n_{H}). Those not reported are initially set at 10^{-20}.

Species	Abundance	Notes
H_2	5.00×10^{-01}	a
HD	1.50×10^{-05}	
He	1.00×10^{-01}	
o-H_3^+	1.80×10^{-10}	
p-H_3^+	3.00×10^{-09}	
N	2.10×10^{-05}	b
CO	1.20×10^{-04}	
O	1.36×10^{-04}	
GRAIN0	5.27×10^{-11}	

[a]The H_2 abundance is distributed between its ortho- and para-forms, depending on the adopted H_2 ortho-to-para ratio.
[b]The abundance of nitrogen corresponds to the total N-reservoir, which we initialised in three different possible ways: fully atomic (N), fully molecular (N_2), or half-atomic/half-molecular (see text for more details).

TABLE 4.2. Binding energies for species that go through time-dependant depletion (see Wakelam et al., 2017).

Species	E_{B} [K]
C	3000
N	720
O	1600
N_2	1100
O_2	1200
CO	1300
NH	2600
OH	4600
NH_2	3200
NH_3	5500
H_2O	5600

4.3.2 The analyzed core

All of our analysis was done applying the post-processing scheme described on Sec. 4.2.2 using the chemical network mentioned on Sec. 4.3.1 on the slow-collapse 'M1' core model case from Bovino et al. (2019).

This core was defined as a Bonnor-Ebert sphere, i.e. a collapsing gas sphere (virial parameter of $\alpha_{\rm vir} = 4.32$), with initial physical conditions being a core mass $M_{\rm BE} = 20\ M_\odot$, along $R_{\rm BE} = 0.17$ pc, a central volume density $n_0 = 1.81 \times 10^5$ cm^{-3}and an average volume density $\langle n \rangle = 2.21 \times 10^4$ cm^{-3}. Also, the core was initialized as turbulent by assuming a Mach number $\mathcal{M} = 3$, and magnetized with an average magnetic field strength $\langle B \rangle = 46\ \mu$G. Its free-fall time is $t_{ff} = 260$ kyr.

The core itself is composed by around $\sim 6 \times 10^5$ gas-particles, yielding a mass resolution of $2 \times 10^{-4}\ M_\odot$, and a spatial resolution of roughly 20 AU.

To keep the post-processing consistent with Ferrada-Chamorro et al. (2021), the gas temperature in the core has been kept constant at 15 K everywhere for most of the runs. Additionally, for three particular runs we have explored CRIR, and temperature as dependent on density, parametrised as will be shown in Sec. 4.3.4.

For dust properties, dust temperature was also settled at 15 K on isothermal cases, while on the density-dependent ones it is calculated separately from $T_{\rm gas}$, Also, a grain material density of 3 g cm^{-3} was assumed, along a dust-to-gas mass ratio of 7.09×10^{-3} and a mean molecular weight μ of 2.4.

4.3.3 Parameter-space exploration

Sipilä et al. (2019) performed several simulations with an exhaustive parameter-space exploration, also including/excluding key chemical processes that could affect the distribution and values of NH_3 abundances. However, this was done using one-zone, pseudo-time dependent models, and they highlighted the importance of modelling chemistry in a dynamic, time-dependent fashion.

With this in mind, and with the aim of exploring the gas-phase and freeze-out chemistry of ammonia and its deuterated isotopologues, exploiting the post-processing method developed by Ferrada-Chamorro et al. (2021), we performed a parameter-space exploration using our expanded chemical network.

In order to probe how the abundance of NH_3 behaves as the conditions of the environment changes, different combinations of other parameters aside the basic structural ones from the core itself were tested, such as CRIR, with values of 2.5×10^{-17} or 2.5×10^{-16}; the H_2 ortho-to-para ratio, or H_2 OPR, set either at 10^{-3} or 0.1 (Lupi et al., 2021) and the radius of the dust grains $a_{\rm gr}$, that could be 0.1 or 0.035 microns respectively.

Finally, different initialisations of the *chemical state of nitrogen*, i.e., whether nitrogen is initially fully atomic (N), fully molecular (N2), or *half-atomic, half-molecular* (N/N2) were also considered.

All of this resulted in 24 distinct isothermal runs, which are summarised in Table 4.3, being F12 our chosen as reference case run, with an average grain radius of 0.1 micron, H_2 OPR = 10^{-3}, CRIR = 2.5×10^{-17} s^{-1}, and a nitrogen initialized as half-atomic, half-molecular. There are also three density-dependent runs, that will be described later on Sec. 4.3.4

TABLE 4.3. List of the performed runs and their associated parameters. The run in boldface is the one that yielded the best fits towards NH_3 column density and deuterium fractionation limits (see text for more details). The *n-dep* label denotes those parameters that has been parametrised to be density dependent as described in Section 4.3.4

Run	Temperature (K)	Grain radius (μm)	H_2 OPR	CRIR (s^{-1})	Nitrogen initialisation
S01	15	0.035	0.1	2.5×10^{-16}	N
S02	15	0.035	0.1	2.5×10^{-16}	N_2
S03	15	0.035	0.1	2.5×10^{-16}	N/N_2
S04	15	0.035	0.1	2.5×10^{-17}	N
S05	15	0.035	0.1	2.5×10^{-17}	N_2
S06	15	0.035	0.1	2.5×10^{-17}	N/N_2
S07	15	0.035	10^{-3}	2.5×10^{-16}	N
S08	15	0.035	10^{-3}	2.5×10^{-16}	N_2
S09	15	0.035	10^{-3}	2.5×10^{-16}	N/N_2
S10	15	0.035	10^{-3}	2.5×10^{-17}	N
S11	15	0.035	10^{-3}	2.5×10^{-17}	N_2
S12	15	0.035	10^{-3}	2.5×10^{-17}	N/N_2
F01	15	0.1	0.1	2.5×10^{-16}	N
F02	15	0.1	0.1	2.5×10^{-16}	N_2
F03	15	0.1	0.1	2.5×10^{-16}	N/N_2
F04	15	0.1	0.1	2.5×10^{-17}	N
F05	15	0.1	0.1	2.5×10^{-17}	N_2
F06	15	0.1	0.1	2.5×10^{-17}	N/N_2
F07	15	0.1	10^{-3}	2.5×10^{-16}	N
F08	15	0.1	10^{-3}	2.5×10^{-16}	N_2
F09	15	0.1	10^{-3}	2.5×10^{-16}	N/N_2
F10	15	0.1	10^{-3}	2.5×10^{-17}	N
F11	15	0.1	10^{-3}	2.5×10^{-17}	N_2
F12	15	0.1	10^{-3}	2.5×10^{-17}	N/N_2
D01	n-dep	0.1	10^{-3}	n-dep	N/N_2
D02	n-dep	0.1	10^{-3}	2.5×10^{-16}	N/N_2
D03	15	0.1	10^{-3}	n-dep	N/N_2

4.3.4 Density-dependent gas temperature and cosmic ray ionization rate

As briefly mentioned before, in addition to the default 24 cases, a non-isothermal gas distribution was also explored. It is important to note that a self-consistent computation of temperature along with hydrodynamics is completely out of the scope of this work.

Instead, to mimic non-isothermal gas dynamics, we employed the self-consistent model for equilibrium gas temperature and size-dependent dust temperature in pre-stellar cores presented by Ivlev et al. (2019). In their work, the authors developed a set of analytical expressions for the gas and effective dust temperatures to be applied to a broad range of physical parameters consistent with cold, dense, prestellar cores. We were able to calculate gas and dust temperatures (T_g and T_d, respectively) as number density-dependent variables for each particle or cell in our simulated prestellar core using these equations, which are dependent on local gas density.

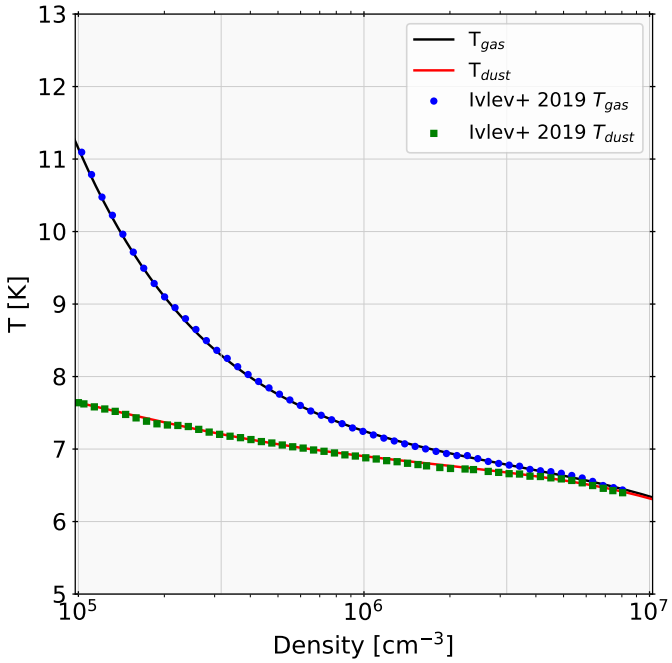

FIGURE 4.2. L1544 pre-stellar core Ivlev et al. (2019) data fitting curves for the T_{gas} and T_{dust} functions defined on Eq. 4.1 and associated relations

To obtain the expressions needed to compute the temperatures, we performed a curve fitting on the L1544 prestellar core data extracted from Ivlev et al. (2019) for both T_g and T_d. This procedure yielded a system of analytical functions that describe the behaviour of these parameters as a function of the hydrogen number density:

$$T_g = \left(a\frac{T_{d0}}{\theta} + b\theta\right)^2, \tag{4.1}$$

$$T_d = T_{d0}\left(1 + 0.202\frac{\zeta_{CR}}{10^{-16}}\left(\frac{T_{d0}}{6}\right)^{-6}\right)^{1/6}, \tag{4.2}$$

with T_{d0} the initial dust temperature, and ζ_{CR} the CRIR. In Eq. 4.1, θ is defined as

$$\theta = (1.7321\sqrt{\mathcal{C}_1} + 9\mathcal{C}_2)^{1/3}, \tag{4.3}$$

where $\mathcal{C}_1$ and $\mathcal{C}_2$ are parameterised as

$$\mathcal{C}_1 = 27\mathcal{C}_2^2 - 4T_{\rm d0}^3, \tag{4.4}$$

$$\mathcal{C}_2 = \left(\frac{\zeta_{\rm CR}}{10^{-16}}\right)\frac{q\,(1+p_2)}{p_1\arctan(q)}, \tag{4.5}$$

with q, p_1 and p_2 coefficients needed to obtain the respective parameters (see Appendix C of Ivlev et al., 2019, for more details on the equations).

The results of the fit are presented in Fig. 4.2, with the black solid line corresponding to the gas-temperature fit, and the red solid line to the dust-temperature fit, while the blue circles and green squares are the gas-temperature data and dust-temperature data taken from Ivlev et al. (2019), respectively.

$T_{\rm d}$ also depends on the CRIR, we derived from Ivlev et al. (2019) an equation to express the dependence of the CRIR on the gas density as

$$\frac{\zeta_{\rm CR}}{10^{-16}} = \alpha n_{\rm H}^{\beta}\exp\left(\frac{-\delta}{n_{\rm H}}\right) + \eta, \tag{4.6}$$

where $n_{\rm H} \equiv \rho/m_{\rm H}\mu$ is the hydrogen number density (with ρ the total gas density and $m_{\rm H}$ the hydrogen mass in grams), and α, β, δ and η are fitting coefficients. It is important to note that these fits are restricted to a similar validity range as the one on the original work, from $10^5 < n_{\rm H}/{\rm cm}^{-3} < 10^7$, to guarantee consistency. In the case our simulation results exceed the density upper or lower limits of this validity range, we impose constant $T_{\rm g}$, $T_{\rm d}$ and CRIR evaluated at the limiting density.

We used these formulae in our code to run three more $n_{\rm H}$-dependent runs: one with density-dependent temperature and fixed CRIR, one with density-dependent CRIR and fixed temperature, and one with both density-dependent quantities, as shown in the last three rows of Table 4.3. All other parameters, such as grain size, initial OPR, and nitrogen initial state are kept at their fiducial values.

Chapter 5

Results

In this chapter we will present the main results obtained during the development of this thesis, in the context of pre-stellar cores inside molecular clouds as presented on Chapter 2, to understand the chemistry on them, following the reaction and processes mentioned in Chapter 3 using the tools described and defined in Chapter 4.

With the goal of exploring the gas-phase and freeze-out chemistry of NH_3 and its deuterated isotopologues under the conditions seen in pre-stellar cores we had included the extended chemical network outlined before on the post-processing framework presented in Ferrada-Chamorro et al. (2021).

In all simulations that will be described later in this chapter, only a fraction $f_{\rm part} = 0.1$ (10 percent) of the total particles that form part of the reference simulation have their chemistry evolved directly, assuming a core-to-background number fraction $\xi_{\rm core} = 0.5\ f_{\rm part}$, while the rest non-directly evolved particles has their chemical abundances via interpolation.

This method has proven to be quite accurate, as in the worst cases, when its results are contrasted with on-the-fly chemistry ones, the discrepancies are around a factor of 2 to 3 only (see Ferrada-Chamorro et al. (2021) for details).

For the analyses we had computed the column densities of ammonia and its deuterated isotopologues, considering the total column density of each species as the summation over all the spin states of said species, by integrating each species number density data cube along the z-axis over a column of 0.2 pc height.

We point out that a part of the results presented here are being used for the development and submission of a scientific publication that at the moment of this thesis presentation is being submitted for a refereed review, expecting it to be published over the next year.

5.1 Isothermal and Constant CRIR cases

We have developed two different yet-related sets of simulations, a group where temperature and density were directly extracted from the hydrodynamical simulation outputs, aka isothermal cases, and other smaller set with temperature and/or CRIR depending on density or n-dependent ones. To start with the results review, we will focus on the isothermal set of simulations first. The chemical evolution was performed across a large parameter-space, already described in Sec. 4.3.3 and resumed in Table 4.3.

The said parameter-space features 24 isothermal runs, with T = 15 K, that we dubbed as either 'S' (small) or 'F' (fiducial), depending on the average grain size used for running them, either 0.035 μm or 0.1μm respectively, varying at the same time several associated parameters at the very beginning. Those parameters are ortho-para ratio (OPR), that can be set to 0.1 or 10^{-3}, CRIR, which is either $\zeta_{\rm CR} = 2.5 \times 10^{-17}$ s^{-1} or $\zeta_{\rm CR} = 2.5 \times 10^{-16}$ s^{-1} and

the initial chemical state of nitrogen, in other words, how is nitrogen distributed between its forms at the start of the simulation, having the possibilities to be settled as fully atomic (Full N), fully molecular (Full N_2) or half atomic/half molecular (N/N_2).

NH_3 evolution under different conditions

We start the analysis of ammonia chemistry under pre-stellar core with its main molecular form, NH_3, by reporting radial profiles at three different times ($t \simeq 50, 100, 150$ kyr) for the eight most relevant simulations in our suite, chosen to highlight the impact of different parameters (Fig. 5.1).

Effect of changing the CRIR: - One really interesting trait that can be immediately noticed when looking at Fig. 5.1 second row (S09 and F09 models) is the direct impact of the CRIR on the results. As mentioned a few paragraphs before, we had employed two different values for CRIR, something that allows us to differentiate the diverse runs in two quasi-distinct groups.

The cases with the higher CRIR initialization ($\zeta_{CR} = 2.5 \times 10^{-16}$) presents a visible boosted abundance, as column density increases by 1 to 2 orders of magnitudes. This is most probably caused by a steady rise of the the cosmic ray-induced desorption mechanism efficiency, that boosts ammonia evaporation rate, surpassing freeze-out process earlier in the evolution, rising abundance to values that are even beyond the range of observations. We note, however, that in our setup we are not including surface chemistry, which can convert ammonia into other solid forms, decreasing the amount which will be returned to gas phase through CR-induced desorption. Though as the core continues evolving depletion signatures start to appear, these signals are pretty mild in the end. In particular, for the F09 run, the profiles at 50 and 100 kyr show the shape observed by Crapsi et al. (2007), with ammonia abundance slightly increasing towards the centre.

However, we point out that here we explored two specific and also extreme cases, that most probably could not be enough to sample all the possible outcomes the evolution could have. Also, it is important to note that very high CRIR values are unlikely to be present and/or measurable in the densest parts of molecular clouds (Padovani et al., 2009) due to the general conditions on these environments.

H_2 OPR effect: - If we look at the high OPR cases (S06 and F06 models), it is possible to see that at larger radii ($r \sim 0.1$ pc), even at the earlier stages of evolution, depletion signatures are present notoriously, and worsen as the core continues evolving, down to a decrease of NH_3 abundance of around $\sim 1 - 2$ orders of magnitude. The resulting abundance slope ends up being completely different, and somewhat the opposite, from the observed one from Crapsi et al. (2007) data.

The effect of varying the H_2 OPR affects the behaviour of ammonia chemistry. Having an initial high OPR (≥ 0.1) value increments NH_3 production efficiency, yielding total abundance larger than a factor of a few compared with observational values. On the other hand, the change in the OPR also shifts the radii at which depletion start becoming relevant to outer parts of the core. Having an small OPR (10^{-3}) causes a great enhancement on the deuteration process efficiency (Harju et al., 2017), boosting deuterated ammonia formation, but decrements regular NH_3 abundance.

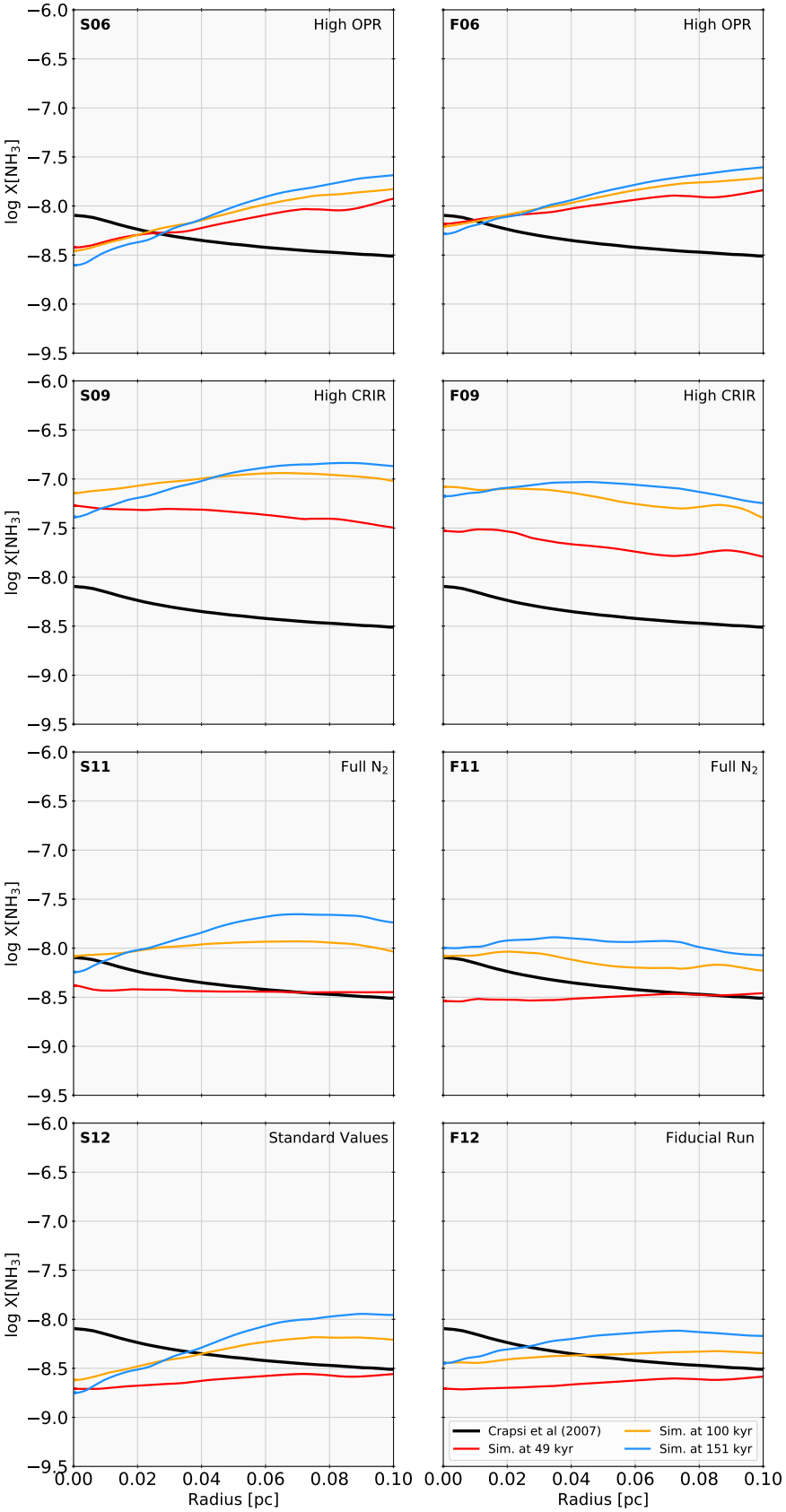

FIGURE 5.1. Relative abundance radial profiles of NH_3 at $t \sim 50$, 100 and 150 kyrs (red, yellow and cyan lines respectively) for High OPR (first row), High CRIR (second row), full N_2 (third row) and Standard modelling values (last row) initializations with grain sizes of 0.035μm (left column) and 0.1μm (right column) compared with Crapsi et al. (2007) NH_3 abundance profile (solid black line).

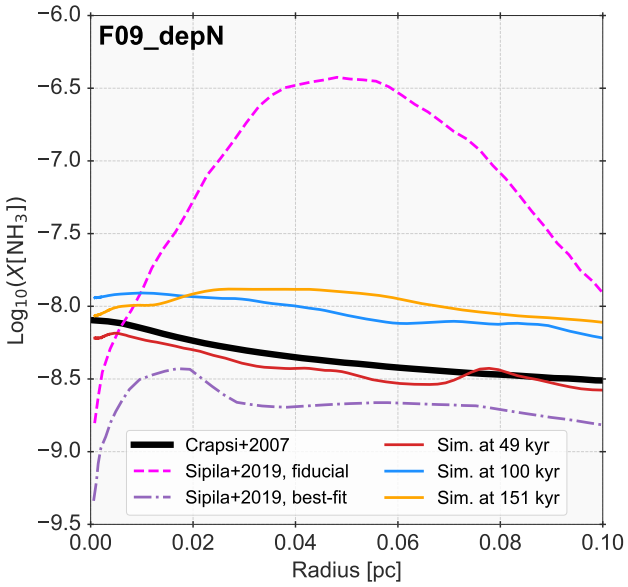

FIGURE 5.2. NH_3 relative abundance profile for the F09_depN run at three different times, compared with the results of Crapsi et al. 2007 and Sipilä et al. 2019.

This is most probably due to the fact that, as shown by Dislaire et al. (2011a), the main gas-phase formation mechanism of ammonia is initiated by the

$$N^+ + H_2 \rightarrow NH^+ + H, \tag{5.1}$$

reaction which heavily depends on the value of H_2 OPR. In their work, Dislaire et al. (2011b) proved that lower H_2 OPR implies, in general, lower ammonia abundances at equilibrium (see their Fig. 3), and this can easily explain the results we got.

GRAIN SIZE EFFECT: - The difference in going from small average grain sizes ($a_{gr} = 0.035$ μm, S-runs), to the fiducial $a_{gr} = 0.1$ μm (F-runs) can be observed by comparing the left column panels 5.1 with their right counterparts. In general, as the grain average size goes smaller, there is a noticeable enhancement of depletion.

This effect can be interpreted as a shift in the critical radius at which depletion becomes dominant over other processes to larger radii (see, for example, S09, where depletion appears at the core's edge at $t = 150$ kyr, and F09, where the abundance peak occurs at $r \sim 0.04$ pc instead).

INITIAL STATE OF NITROGEN: - The last parameter that we took into consideration to study ammonia chemistry evolution under pre-stellar core conditions and that is in need of review for this purpose is the initial chemical state of nitrogen. Interestingly, the initial state of N has a dual effect. On one hand, it slightly boosts the total abundance of ammonia. On the other hand, it tends to slow down the depletion rate, as can be seen in S11 and F11, where the abundance profiles remain almost flat for the initial ~ 100 kyr (in the S11 case) or even over the entire simulation time of ~ 150 kyr (in F11).

In general, if we start only with atomic N, ammonia abundances are low at the very end. The main reason behind this is that NH_3 highly depends on the amount of N_2 available to form it, and, as N_2 formation from atomic N is known to be a really slow process involving several neutral-neutral reactions (Nguyen et al., 2018), there will be less N_2 available to form

ammonia, and thus depletion will begin much later. However, due to the physical conditions in dense, pre-stellar cores, it is not expected to find nitrogen purely in atomic form.

Additionally, we could see that the F09 observed profile slope is in really good agreement with Crapsi et al. (2007) one, with slightly higher abundances at all times. As this happened, we decided to make an additional test variation of the F09 model in which the initial abundance of nitrogen in the system was set at just 10% of the fiducial nitrogen abundance (i.e., nitrogen is initially depleted). We named this new run F09_depN, and we show its radial profiles in Fig. 5.2, comparing our results to Crapsi's as a black line, as well as the fiducial model and best-fit model from Sipilä et al. (2019) for NH_3. In this case, the agreement with the observed profile by Crapsi et al. (2007) improves significantly at all times, with more coincidence between the results at the early stages of evolution.

NH_2D evolution under different conditions

As this work is about ammonia and its deuterated isotopologues chemistry evolution in pre-stellar cores, we also present the results of our post-processing for the same selected runs as the previous case of NH_2D in Fig. 5.3.

In general, we have close to flat profiles, as seen in almost all of the cases in this figure, with the exception of determined time-steps on specific runs, and there are no high column density variations as time passes over the simulations, at least in the central region of the core. When we look at high H_2 OPR cases, we see the lowest abundances of all the runs shown on Fig. 5.3, with slopes that range from quite flat to increasing towards the center (from r $\sim$ 0.5 pc in F06), and abundances that increase by roughly one order of magnitude within the core evolution. This behavior is noticeably different from the NH_3 results for the same run, but these differences are not translated in the other runs.

If we set a High CRIR value, the most visible feature here is a high enhancement on column densities, with an increasing toward the center. The increase in abundance over time is less than one order of magnitude between each time step considered, with some little signs of depletion appearing at $t\times$ 150 krys in the S09 case. These results are very similar to their NH_3 counterparts, confirming that high CRIR values boost ammonia evaporation from dust grains, increasing its abundance and decreasing freeze-out effects.

Now, comparing the cases with low a_{gr} with the ones having fiducial a_{gr}, it is possible to see that both possibilities have really similar abundances, with a_{gr} = 0.035 μm having very slightly higher values in general, but also presenting a lower degree freeze-out on S cases when the evolution time of the core reaches $t \sim$ 150 krys.

Lastly, when we explore the effect of nitrogen initialization, we do obtain similar results in terms of slopes, with a higher abundance shift between the first control time-step and the second one than in the other cases (especially in F11), but a very low change in the time range between 100 and 150 krys. As seen in our profiles, this can be explained by the expectation of an increase in the production of Ammonia species molecules as more molecular nitrogen becomes available for the process.

We can conclude that some parameter variations have a similar effect over NH_3 and NH_2D, as when a high CRIR value is used, supporting the conclusions obtained for this parameter on regular ammonia. However, there are also some differences, as this particular species presents almost no freeze-out traits, mostly at late evolutionary stages, due to some column density enhancements that act against it.

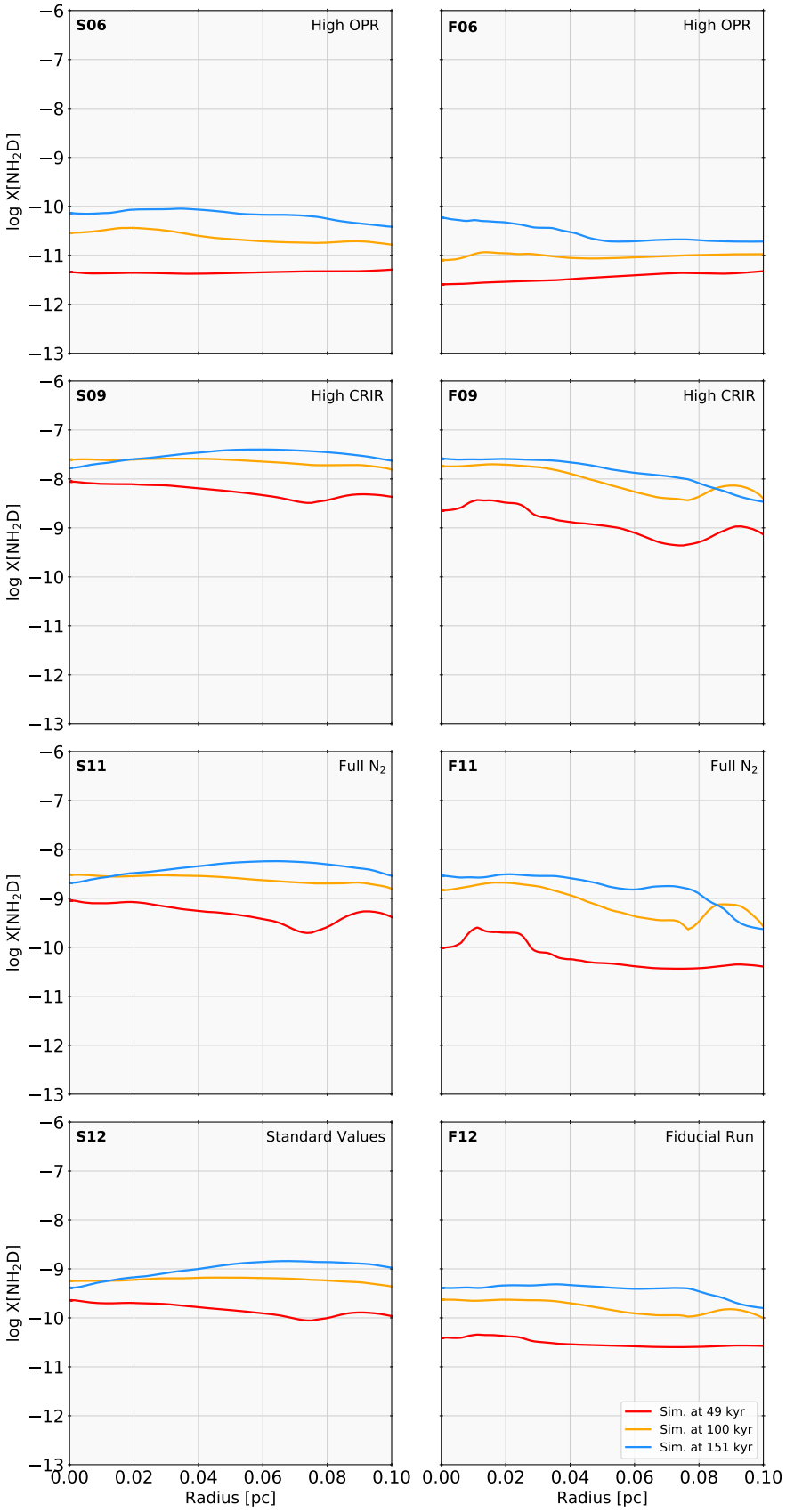

FIGURE 5.3. Relative abundance radial profiles of NH_2D at $t \sim 50$, 100 and 150 kyrs (red, yellow and cyan lines respectively) for High OPR (first row), High CRIR (second row), full N_2 (third row) and Standard modelling values (last row) initializations with grain sizes of 0.035μm (left column) and 0.1μm (right column).

NHD_2 evolution under different conditions

As we continue our analysis of deuterated ammonia isotopologues, we must review the case of the doubly deuterated form, NHD_2, the results of which are presented in the same manner as the previous ones on Fig. 5.4.

One of the first things we point out here is that, in general, the abundances of this form of ammonia are around a half to an order of magnitude lower than the previous cases. This is most probably a consequence of deuterium being a very small fraction of the total available hydrogen. Furthermore, with the exception of a very small region (0.1 pc) on cases with larger grain size, almost all cases show increasing abundances toward the center.

Once again, high-CRIR cases demonstrate the highest abundance among all the shown cases, with very light changes along the whole core evolution. similarly to what had been seen on the other two isotopologues.

When we look at the high OPR runs, we can see that they begin with nearly flat profiles, indicating that NH_2D and NHD_2 have similar column density coefficient values with just different orders of magnitude but much lower abundances than the regular ammonia set of simulations. The abundance of NHD_2 increases dramatically as it evolves, ~ 3 orders of magnitude, with profiles growing to the center of the core close to the edge in the small grain size case (S06) and around $r \sim 0.5$ pc in the standard grain size run (F06).

For the initial chemical state of nitrogen, when looking at the case initialized as fully molecular (i.e. full N_2), the obtained results are similar to the case with high CRIR, but with a lower abundance.

Here, we can conclude that NHD_2 chemistry is not too much altered depending on the environmental parameters, except for the ortho-para ratio, which quietly reduces the initial abundance of the molecule, but also enhances its production over time, varying the radius where this abundance augment starts to be more relevant depending directly on the average grain size more than any other parameter.

ND_3 evolution under different conditions

Finally, now that we have examined all other forms of ammonia, we can present the results for the last variant: the fully deuterated ammonia molecule (ND_3). The results are obtained and shown under the same conditions and for the same cases as NH_3, NH_2D, and NHD_2, as can be seen on Fig. 5.5.

All of these cases have lower abundances than the other isotopologues, especially for the high OPR cases. In the particular case of high CRIR, the column densities grow by about 5 orders of magnitude, with around two orders of magnitude jumps between each time step. In both small and regular grain sizes, the profiles have an increase towards the center slope, with a small depletion feature at $t \sim 100$ kyrs on the most central parts of the core. There is an abrupt increase in abundance around $r \sim 0.5$ pc for F06 and the outer edges for S06 at $t \sim$ 100 kyr in the cases with higher OPR (S06 and F06).

The results for the remaining conditions, as seen in Fig. 5.5, are consistent with the NHD_2 ones, with a general increase toward the center independent of grain size, small abundance changes over time when $a_{gr} = 0.035$ μm, and a large abundance jump from t $\sim$ 50 to 100, but a small one between t $\sim$ 100 to 150 krys when $a_{gr} = 0.1$ μm.

Our conclusions for this particular isotopologue are very similar to those for NHD_2, in that the slopes of the abundance profiles do not change much as we change the different parameters, except when we consider a high OPR, with a higher abundance increase over

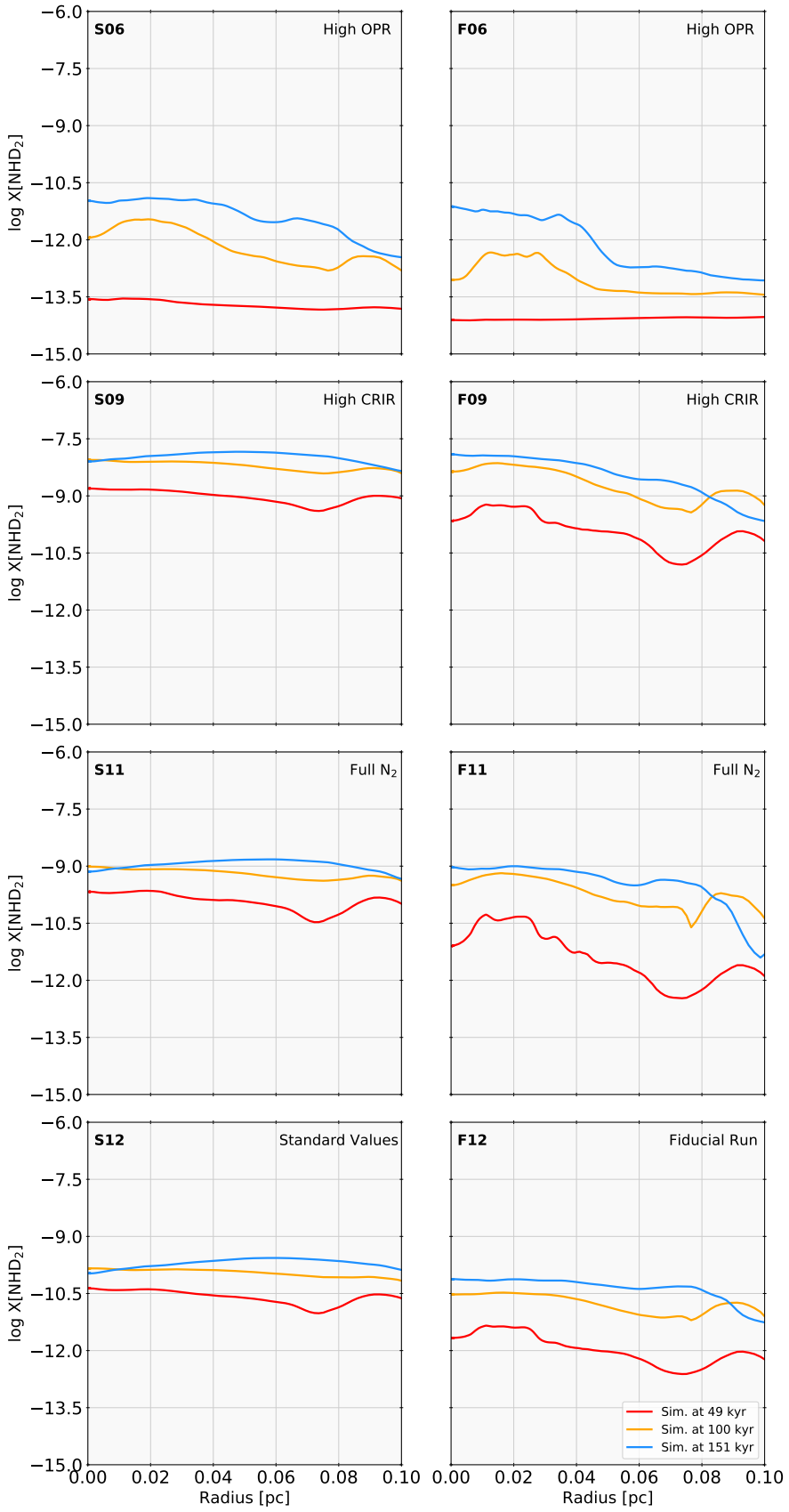

FIGURE 5.4. Relative abundance radial profiles of NHD_2 at $t \sim 50$, 100 and 150 kyrs (red, yellow and cyan lines respectively) for High OPR (first row), High CRIR (second row), full N_2 (third row) and Standard modelling values (last row) initializations with grain sizes of 0.035μm (left column) and 0.1μm (right column).

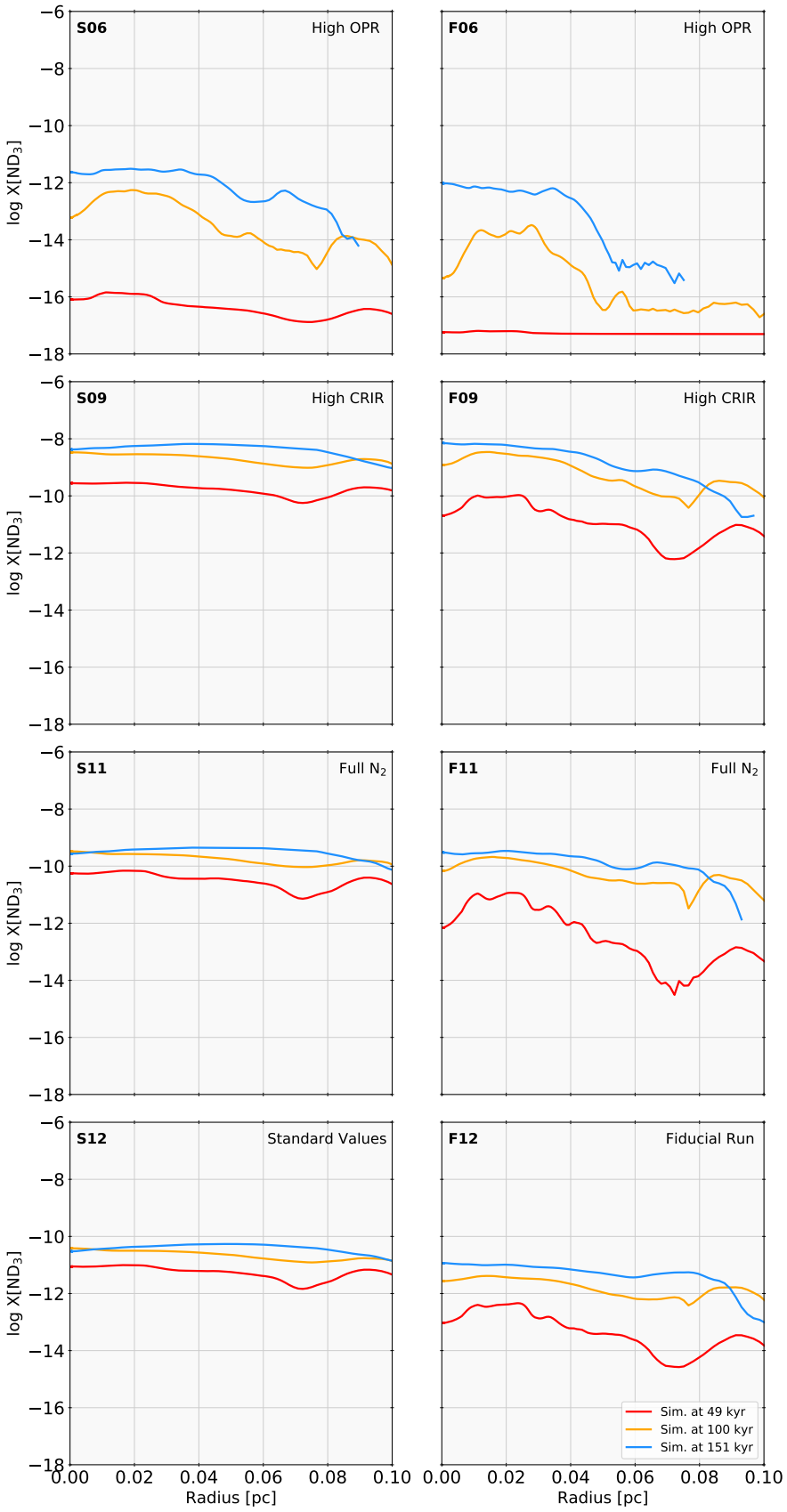

FIGURE 5.5. Relative abundance radial profiles of ND_3 at $t \sim 50$, 100 and 150 kyrs (red, yellow and cyan lines respectively) for High OPR (first row), High CRIR (second row), full N_2 (third row) and standard modelling values (last row) initializations with grain sizes of 0.035μm (left column) and 0.1μm (right column).

time than the one seen in the NHD_2 case.

After we had reviewed all the forms of ammonia molecules, we can conclude that, in general, the different parameters we explored have a weak role in regulating the depletion of ammonia in the innermost regions, which, contrary to what was expected from current observations ((Pineda et al., 2022)), is either very mild or not present at all. The profile normalization, however, exhibits strong variations among the eight selected runs, suggesting that the parameters can have a strong impact on the total amount of ammonia formed in the core, especially in the CRIR case, which in all cases presented an enhancement in abundances.

Surprisingly, and contrary to our expectations, our reference run F12, which had all its parameters set to standard values, does not exhibit the best agreement with the Crapsi et al. (2007) behavior we had as a reference, but rather F09 (and its nitrogen-depleted version, F09_depN).

We also see that, while NH_3 exhibits slight depletion features in a few runs, in the at least singly deuterated ammonia cases, we got almost only increasing in the center and a general increase in the production of deuterated ammonia molecules over time.

5.2 Effects of density-dependent temperature and CRIR

All the results presented in the previous section were obtained under isothermal conditions. Even with these considerations, the results presented so far are diverse, yet present some common traits for almost all runs that share certain parameters, suggesting that specific conditions can significantly affect the observed features on any studied core in a similar way as we do here.

The NH_3 abundance profile from Crapsi et al. (2007), is well recovered in some of our isothermal runs (S09, F09, F11, and F12, for example), with minor shifts at later stages of the simulated core evolution. In any case, there are many aspects that our isothermal simulations cannot capture; for instance, any dependence on the temperature is completely neglected in this approach. So, using the methodology detailed in Section 4.3.4, we aim to give a brief look at the effects temperature has on the ammonia abundance. We also look at the effects of CRIR using a similar density-dependent method to further probe the effect of this parameter on the results.

Along with the 24 isothermal runs we produced, some of which were already addressed above, we made three additional runs dubbed as 'D' (**D**ensity-**D**ependent). These runs had their parameters initialized as follows: F09 conditions with T_{gas}, T_{dust} and CRIR depending on density (D01); F09 conditions with T_{gas} and T_{dust} being n-dep (D02); and a last case with F09 conditions having an n-dep CRIR (D03).

The density dependent distributions for the gas and dust temperature, and the CRIR are shown in Fig. 5.6. Here we show some integrated intensity maps obtained in our D01 model at $t \sim 50$ kyr (left column) and $t \sim 100$ kyr (right column). As shown in the figures, all three parameters have spatial distributions that closely follow the gas density, as expected.

Then, with the density-dependent scheme working, we can now go on to see how ammonia abundance behaves, as we did for our isothermal runs, going through each ammonia isotopologue once again.

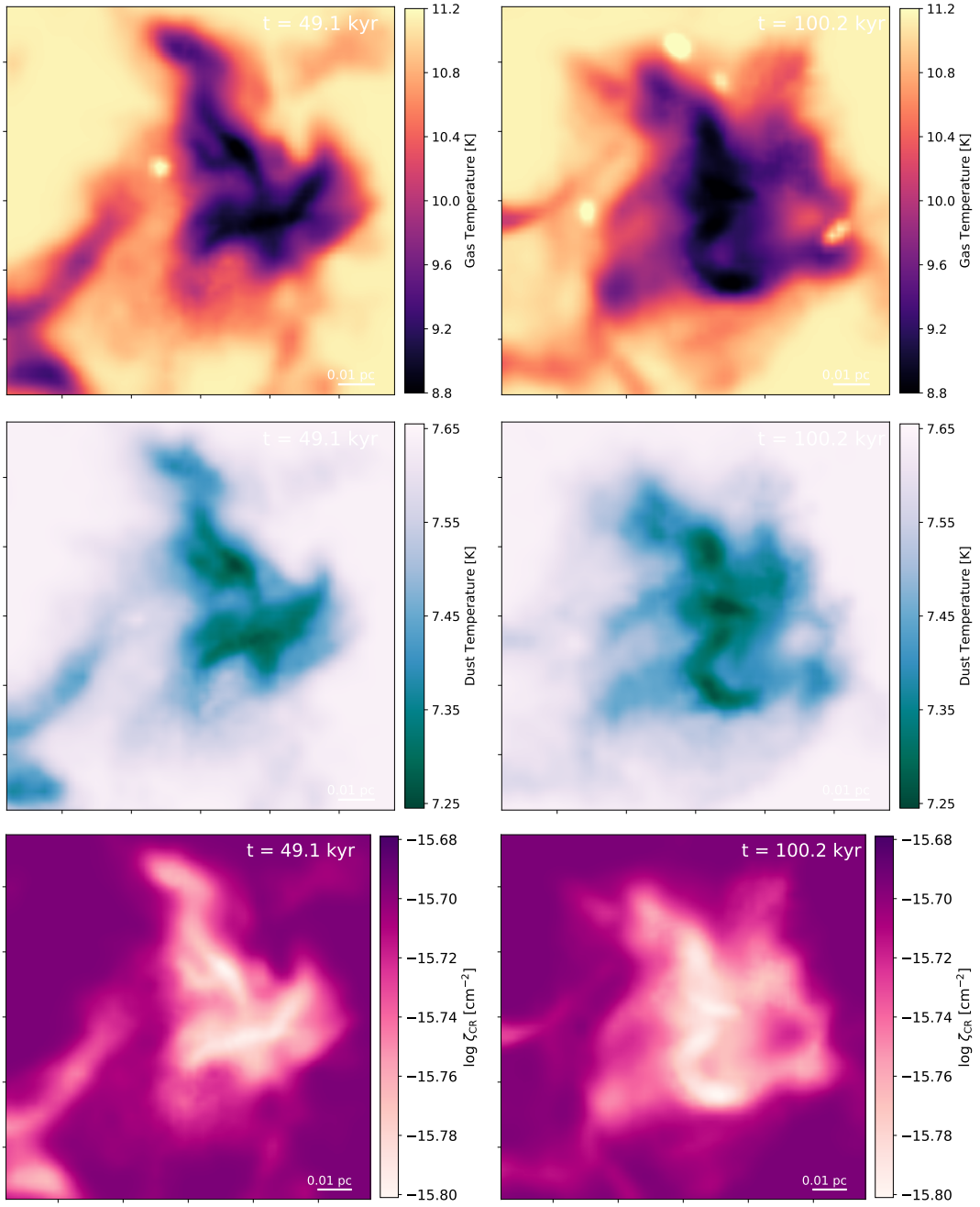

FIGURE 5.6. Distribution of Gas Temperature, Dust Temperature and CRIR maps for D01 non-isothermal model at $t \sim 50$ kyrs (left) and 100 kyrs (right)

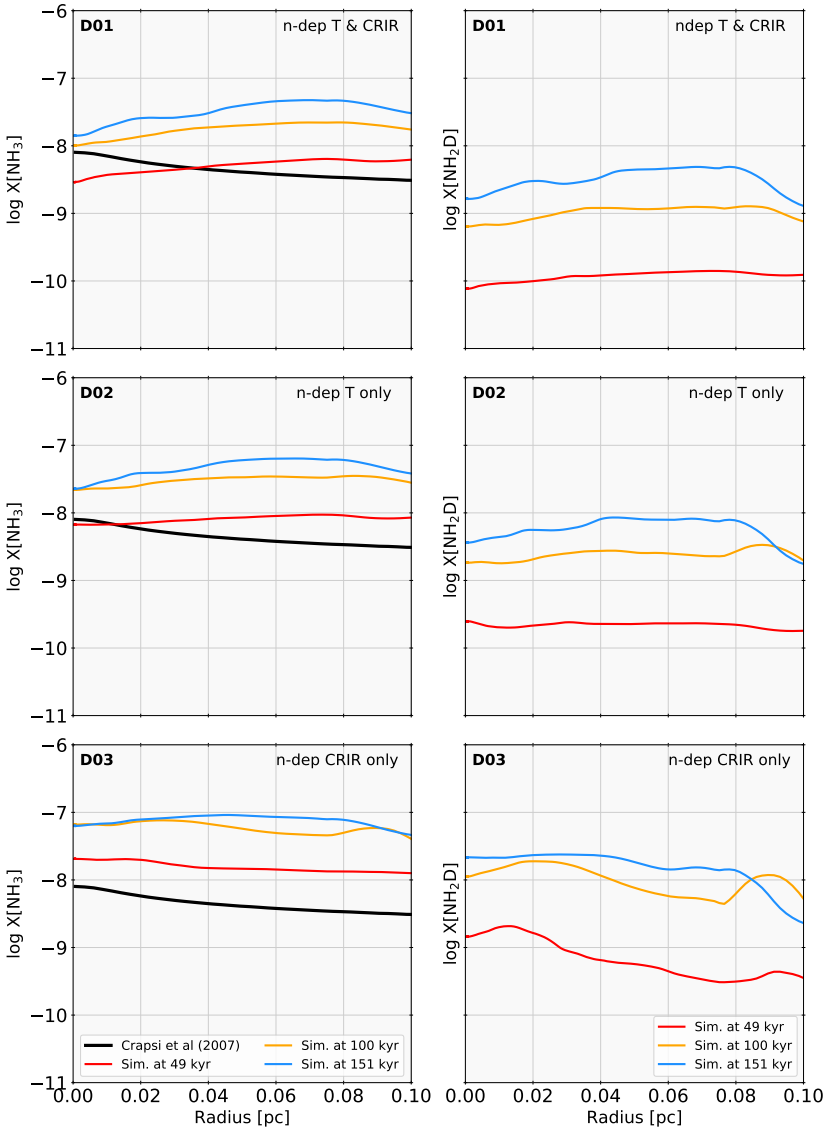

FIGURE 5.7. Relative abundance radial profiles of NH_3 and NH_2D at $t \sim 50$, 100 and 150 kyrs (red, yellow and cyan lines respectively) for T_{gas}, T_{dust} and CRIR depending on density (top), T_{gas} and T_{dust} being n-dep and fixed CRIR (middle) and n-dep CRIR with fixed T = 15 K, (bottom). In NH_3 cases, they are also compared with Crapsi et al. (2007) abundance profile (solid black line).

The case of NH_3

We present the results for NH_3 for each of the three D models in the left column of Fig. 5.7, comparing them to the observed profile in Crapsi et al. (2007), as we did for our isothermal cases in Fig. 5.1.

For Model D01 (top left panel), we can see some mild depletion features towards the center of the core, with almost the same slope at each time step, with different orders of magnitude. Despite this, the total abundance of ammonia grows by around one order of magnitude as evolution continues, with values that are in agreement with Crapsi et al. (2007). The behavior of this model does resemble that of the isothermal runs, which have the most similar initialization compared to it (F09 and F12), but with a slight enhancement in column densities compared with them.

If we remove the density dependence from CRIR, keeping it constant at $\zeta_{CR} = 2.5 \times$

10^{-16}, leaving only gas and dust temperature (Model D02, in the middle left panel), the results do not differ significantly from the D01 case, except for a slightly higher abundance of NH_3 at all times, implying that CRIR plays a secondary role and temperature distribution are more important in affecting the chemical evolution of both D01 and D02.

To understand the influence of CRIR on this case, we kept density-dependent CRIR alone, fixing T at 15K (Model D03, bottom left panel). This case is distinguished by an early moderate increase in NH_3 abundance towards the center, similar to that observed in Crapsi et al. (2007), but with a higher total abundance. This behavior is preserved until the core's very last evolutionary stages, when very subtle signs of depletion appear. This run has a lot of similarities with F09, which is not a surprise as, except for the density dependence on CRIR, both runs have the same initialization parameters, which once again tells us about the impact CRs have on reducing NH_3 depletion.

The case of NH_2D

Now we shift our attention to the singly deuterated ammonia molecule (NH_2D), the results of which are shown in the right column of Fig.. 5.7.

In general terms, the results for this isotopologue in the models with density-dependent temperature (D01 and D02) almost mimic the behaviour of their regular ammonia counterparts, but with an overall lower abundance at all times, which is expected, and presenting a higher jump in column densities from one time-step to another.

On the other hand, for D03, there can be seen some small signs of depletion near the center of the core at $t \sim 50$, which moves a little to the outer part at $t \sim 100$ kyr. This completely disappears when we are close to the end of the simulation, contrary to ammonia, which begins with a soft increase in the center profile and later depletes it at advanced evolution time-steps.

When compared to the corresponding isothermal cases, F09 and F12, all D cases for NH_2D behave similarly to their NH_3 counterparts, though abundances appear to be a little more spread out, with D03 having the most similar one.

The cases of NHD_2 and ND_3

For the last part of this ammonia chemical behavior review, we will dive into the last two ammonia isotopologues, NHD_2 and ND_3, whose results are shown in Fig 5.8. We will review them both together due to the high degree of similarity seen between them, especially when we look at the D03 profiles for those species.

In particular, in D01 cases, both isotopologues present very similar abundance trends at each time step, starting quasi-flat and very slowly decreasing to the center. When the core evolution reaches $t \sim 150$ krys, both species present a high increase (more than a half order of magnitude for NHD_2 and over one and a half orders of magnitude in the case of ND_3) until we reach around $r \sim 0.9$ pc from the center, then start to decrease very slowly towards it.

Then, for the D02 model, we see very similar results as we did for the D01 model, with some small changes. When t is $\sim$ 50 krys, the column densities for both species almost completely increase to the center rather than flattening, whereas later times, the slopes are flatter than in the fully n-dep modeling.

Finally, the D03 model results for each case are nearly identical, with a slightly lower abundance of ND_3. The column densities appear to be increasing toward the center until

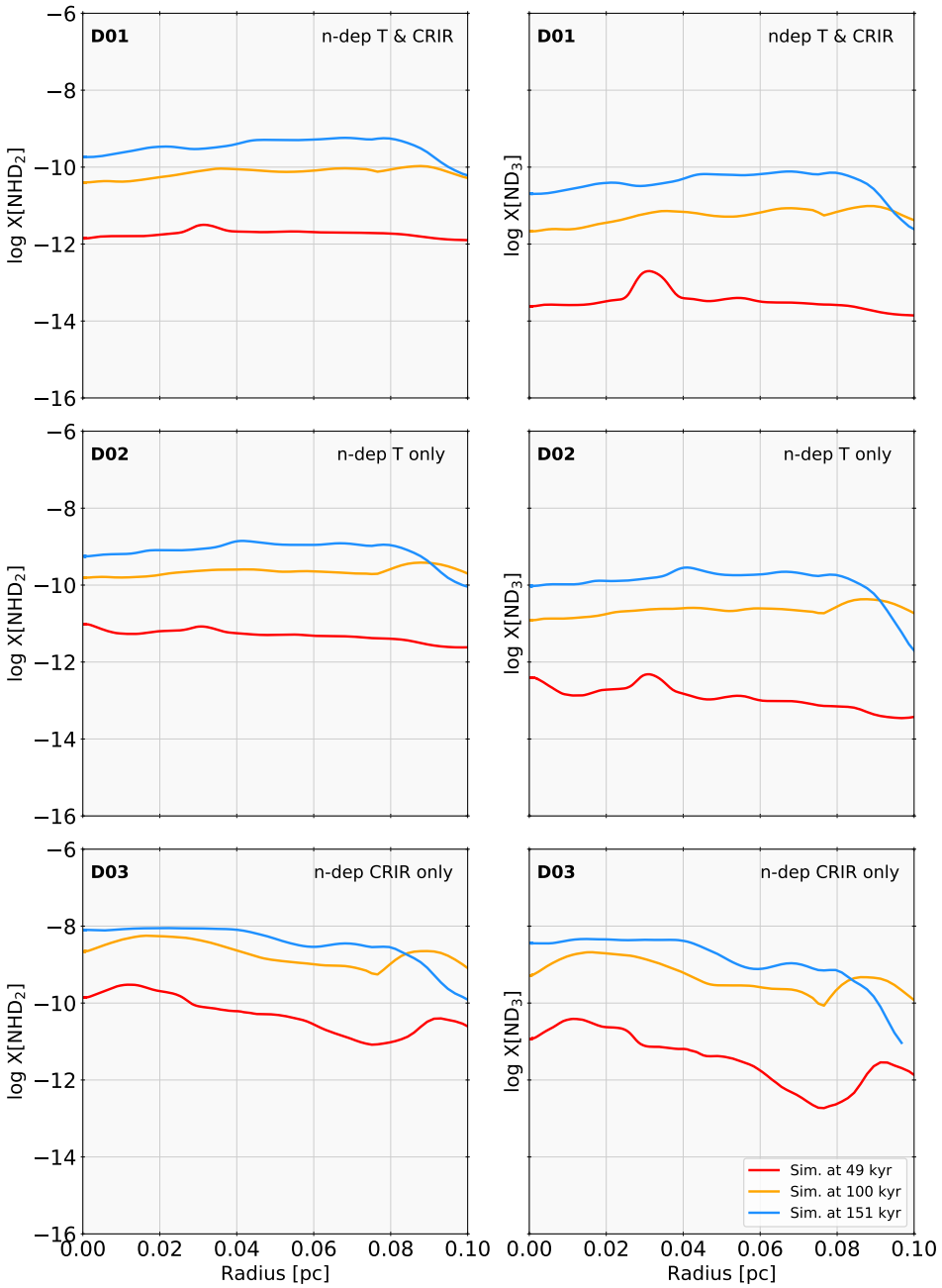

FIGURE 5.8. Relative abundance radial profiles over time of NHD_2 (left) and ND_3 (right) at $t \sim 50$, 100 and 150 kyrs (red, yellow and cyan lines respectively) for T_{gas}, T_{dust} and CRIR depending on density (top), T_{gas} and T_{dust} being n-dep and fixed CRIR (middle) and only n-dep CRIR with fixed T = 15 K, (bottom)

the very central part of the core, where they present a very mild depletion feature at early and in the middle evolution times. The abundance slopes then flatten at the very end of core evolution.

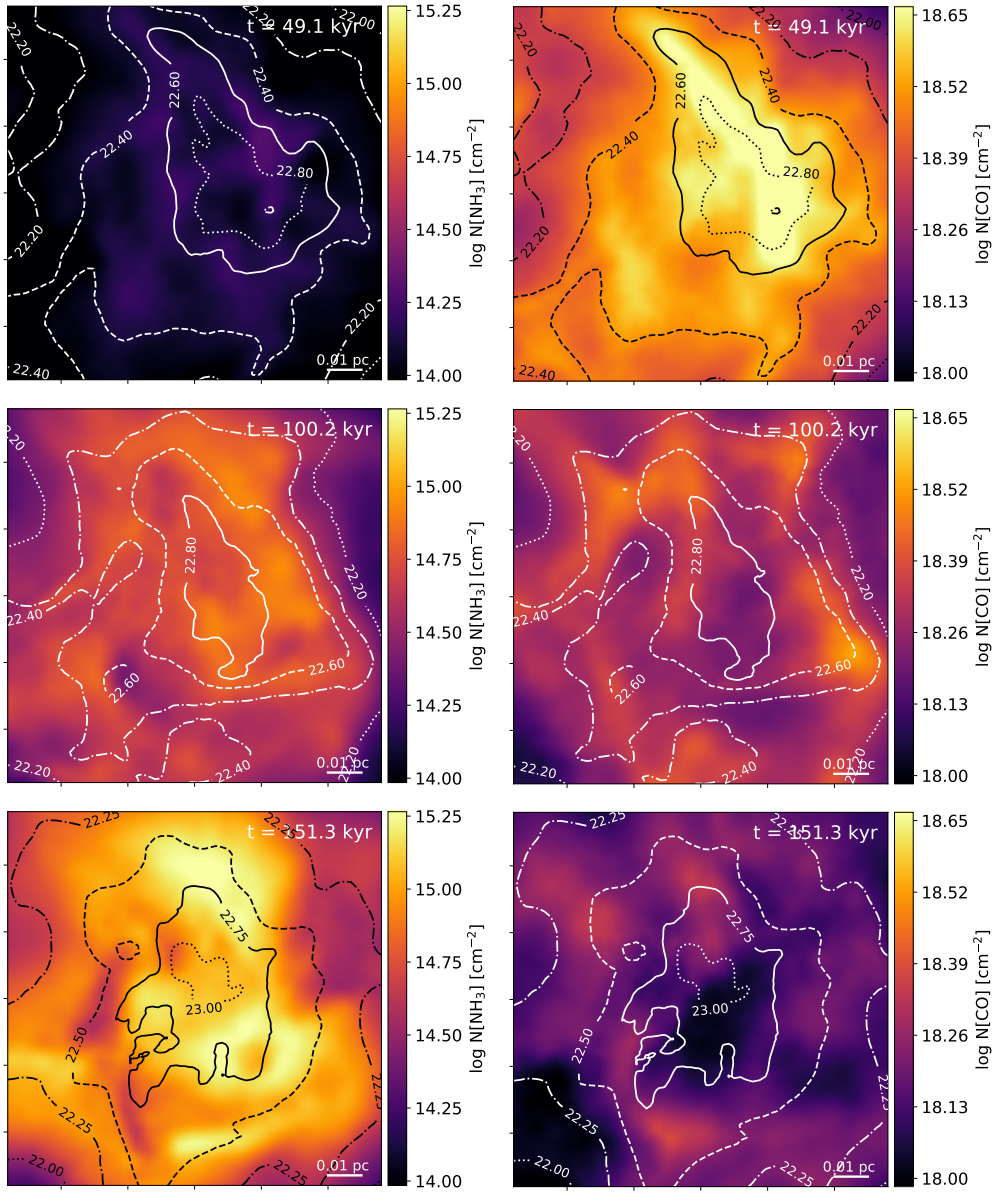

FIGURE 5.9. Maps of NH_3 (left) and CO (right) column density distribution for D01 model with total column density contours overplotted at $t \sim$ 50, 100 and 150 krys.

Comparing all cases for these isotopologues with the isothermal runs, the only ones that have some resemblance to them are the D03 runs. This implies that the temperature of gas and dust has a stronger influence than the CRIR on these species' abundances, as those temperatures counterbalance the abundance increase caused by high CRIR values, similarly to what happened for the other ammonia isotopologues as well. and also enhanced depletion into dust grains.

In addition to all the results presented above and to have a clearer idea of how ammonia distributes in our simulations, we made some column density maps of NH_3 (left column) and CO (right column, chosen for depletion comparison purposes) with total column density

contours over-plotted for the non-isothermal D01 model at the same three time-steps used on the radial profiles, as can be seen on Fig. 5.9.

If we focus on NH_3, we can see that it does not follow the total column density distribution over time, with its abundance increasing over time, but this increase is not as strong in the simulated core center's surroundings as it appears to be on the outskirts. On the other hand, if we look at CO, it starts with a high abundance value, following almost perfectly the total column density distribution over all the core evolution, but its presence heavily diminishes in general, but more especially towards the core center. We can conclude that contrary to CO which is highly depleted in the center of the core, ammonia seems to go over a smoother depletion process, where the peak of depletion is observed off-center.

Adding those maps to the previous results and the different cases we had tested and reviewed in this work, in several of our runs we obtained some profiles for ammonia that shared a lot of similarities with Crapsi et al. 2007 one.

A general conclusion we can deduce from the density-dependent runs is how the resulting profiles highlight the important role temperature distribution has on ammonia evolution, which is more heavily affected when compared to other parameters such as CRIR. Also, we can conclude, that a high CRIR value could enhance the production of all ammonia isotopologues, yet having a CRIR at these levels is really difficult under pre-stellar core conditions.

Chapter 6

Concluding Remarks

We used an up-to-date chemical post-processing scheme on a 3D-MHD simulation of a slow collapsing pre-stellar core, taking into account an accurate treatment of the dynamics of the collapsing star-forming region yet focusing only on its well-known gas-phase chemistry and classical thermal and non-thermal desorption processes. Our aim was to recover the observational non-depletion behavior of ammonia and its main deuterated isotopologues as presented in Crapsi et al. (2007) and several other works.

We have shown here that ammonia chemistry evolution in pre-stellar cores depends on several parameters, such as the H_2 ortho-para ratio, average grain size, and CRIR, yet the influence level of some of them is quite mild. In particular, we found that although the temperature of gas and dust do not play a major role in ammonia chemistry evolution, neglecting their influence could lead to erroneous estimations of ammonia depletion levels.

6.1 Discussion

6.1.1 Comparison with up to date observations

Most of our work was developed around the results from Crapsi et al. (2007), that is more than a decade old at the moment of this thesis writing.

When we started the simulations whose results are presented in Chapter 5, several works tried to address *the ammonia non-depletion problem*, in both theoretical and observational ways, but none of these more up-to-date works was conclusive enough to validate or deny Crapsi's findings. During the run of the year 2022, there were two publications, Caselli et al. (2022) and Pineda et al. (2022) that presented new observational results for ammonia abundance in pre-stellar core conditions. In both cases, they obtained results partially contradictory with Crapsi et al. (2007), especially Caselli et al. (2022).

As most of our simulations were done trying to replicate Crapsi et al. (2007) results with more modern tools, the possibility that our findings could not match these newest observations exists. As a result, we must double-check if our results are consistent with those works, keeping in mind that the differences in approaches between theirs and ours may result in some discrepancies.

In this section, we look at how these more up-to-date observations compare to our results, in a qualitative more than quantitative way, testing how accurate our framework appears compared to them.

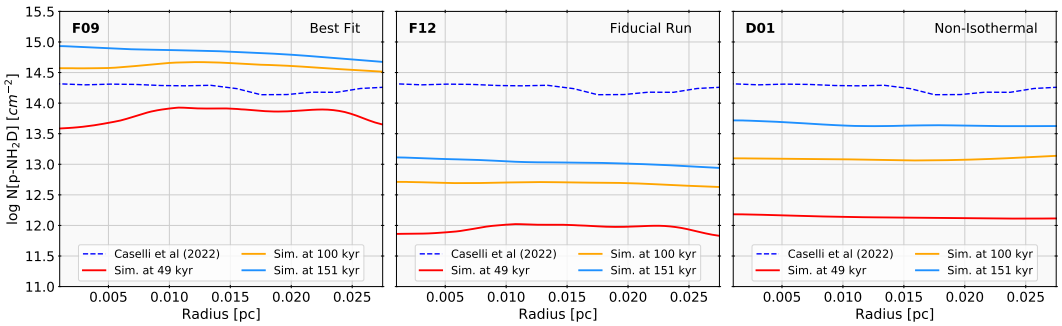

FIGURE 6.1. One time deuterated Ammonia (p-NH_2D) column density radial profiles at t = 49, 100 and 151 kyrs (red, yellow and cyan lines respectively) for our best-fit model (F09, left panel), fiducial run (F12, middle panel) and non-isothermal and n-dep CRIR model (D01, right panel) compared to Caselli et al. (2022) p-NH_2D column density profile (blue dotted line).

Comparison with Caselli et al. (2022)

A recent publication with similar goals as this thesis is Caselli et al. (2022), where the authors reported interferometric observations with ALMA along with chemical modeling over the prototypical low-mass prestellar core L1544. Both the observations and the models they built to test the observations revealed ammonia depletion, particularly for the deuterated isomer p-NH_2D, as seen near the center of the studied core, on a compact region with a radius of around $\sim$ 1800 AU known as the *kernel* identified as the main cradle for the said stellar system.

With their data analysis, they concluded that, due to the high fractional abundance of p-NH_2D on the edges of the *kernel* itself, it was nearly impossible to have a complete and/or clear view of the freeze-out effect inside this layer without high enough angular resolution. This was the main reason why this behavior could not be cleared previously. The effects of depletion on the inner part of this *kernel* are quite high, so they predict that as the core continues evolving and starts forming stars, it will be inevitable that most heavy molecules end up trapped in ices one way or another.

Although the aforementioned work and ours have pretty different approaches, in the end, we could resolve similar scales with our modeling as we have a similar resolution, so we can compare our results against the ones they obtained, both qualitatively and quantitatively.

To make a meaningful comparison, we have calculated column densities of p-NH_2D for our best-fit model, F09, i.e. the model where the NH_3 profiles closely reproduce the observations reported by Crapsi et al. (2007); our fiducial model, F12; and our main non-isothermal model, D01, on the same three timesteps as the previously shown radial profiles, and contrasted them to the column density profile they observed for p-NH_2D, presented in Fig. 6.1.

As shown in Fig. 6.1, presented as the blue dashed line on each panel, they obtained a nearly flat column density profile with a value of 2×10^{14} cm $^{-2}$ from the center to the outer parts of the L1544 cloud, decreasing slightly as they moved out of kernel influence. Their results are not so different from any of our chosen comparison cases. Note that once calculated the abundances, the center will show depletion, as the H_2 column density will increase toward that region.

In the particular case of our best-fit model, F09, presented on the left panel of the aforementioned figure, is the one that better agrees with Caselli et al. (2022) results, showing

similar column density values with a slightly reduced presence of p-NH_2D on the central parts of the core at early evolutionary stages. On the other hand, F12, on the central panel, and D01, on the right panel, also present near-to-flat behavior column density profiles, closer in shape to Caselli et al. (2022) one, but with a notable order of magnitude difference. F12, in particular, appears to underestimate the presence of p-NH_2D by two to three orders of magnitude depending on the evolution of the core, but the distribution is consistent with the observations. Finally, when we address D01, we get a very similar trend to F12, with a larger magnitude difference between steps but also a closer match to the observational data than our fiducial run.

Wrapping up this comparison with the results presented on Chapter 5, some things arise: First, as seen in Sec. 5.1, our best-fit model almost mimics Crapsi results for NH_3, while acting well when we compare the column densities we obtained to up-to-date observations of singly deuterated ammonia, which validates our working scheme for that model.

In the case of our fiducial run, while the absolute amount of NH_3 and NH_2D are not in line with existing observations Crapsi et al. (2007) and Caselli et al. (2022), it replicates quite well the behavior of both ammonia isotopologues.

Finally, in the representation of the non-isothermal modeling scheme, when comparing D01 to observations, we get some slightly improved results concerning our isothermal fiducial run. This means that although our non-isothermal approach is quite simplistic, with some refinement, this modeling scheme can be very useful for more realistic representations of chemical evolution.

6.2 Conclusions

6.2.1 In relation to recent Theoretical works

One of the main reasons we had to perform all the simulations we presented in this work was the noticeable differences between Crapsi et al. (2007) and almost all theoretical works that tried to emulate its results over the years. All the existing model indeed are based on low-dimensionality schemes.

Some existing state-of-the-art low-dimensional models, as (Sipilä et al., 2019), had shown very high depletion towards the center ammonia abundance results, even on its best-fit models, as can be partially seen on 5.2 pink and purple line.

For this work, it is notable that in all the tests we performed, even the worst ones, we observed mild depletion, which contradicts what was reported in recent works Sipilä et al. (2019). This confirms once again that these kinds of simulations need to be done with a three-dimensional structure of the core, along with a proper treatment of turbulence and the magnetic field, which are fundamental to describing the evolution of star-forming regions.

6.2.2 Observational features

The main objective of this work was to understand the phenomena that produced the ammonia abundance profile presented by Crapsi et al. 2007 and try to replicate it using an extensive parameter space on an up-to-date modeling scheme, as well as alleviate in some way the known discrepancies between models and observations of this particular species.

Changing simple parameters such as the H_2 ortho/para ratio, the CRIR, the temperature of gas and dust, and the nitrogen initial distribution have small effects on ammonia depletion. It is important to note that these parameters modify ammonia abundances in quite specific ways that are preserved across all ammonia isotopologues, while some other traits are only valid for deuterated variant species.

In particular, based on our results, we can say that having high CRIR values leads to a rise in the abundance of ammonia and its isotopologues when compared to more standard values. In the case of the ortho-para ratio, the most visible change it causes is a drift in the radii where depletion becomes important.

While a few runs deviated significantly from the observed results, the majority of our runs agree very well with Crapsi et al. (2005) for NH_3 and Caselli et al. (2022) for p-NH_2D within typical prestellar core conditions, particularly when high ζ_{CR} values are assumed. Our modeling scheme works well when replicating results from more recent works, particularly when comparing ammonia-deuterated isotopologues.

We also have shown results for the other isotopologues of NH_3, which, as can be seen, present similar responses to the ones for which we have observational results available.

It is important to note that the comparisons between our results and observations are mostly qualitative, and that in the case of applying a proper radiative transfer or telescope-like convolution, the column densities are expected to be lowered by at least 30%.

6.2.3 Density dependence Implementation

Most previous theoretical works did not or just partially take into account the effect that a non-isothermal scheme could generate on the chemistry evolution under pre-stellar core conditions, so we tried to give a simple look at implementing a density dependence on gas and dust temperature while also doing it for CRIR.

Having this density dependence on the gas and dust temperatures alone or paired with a density-dependent CRIR tends to strengthen depletion effects towards the center of a pre-stellar core. On the other hand, having a density-dependent CRIR profile alone appears to reduce depletion signatures on ammonia, especially at the early stages of evolution, reaffirming the trend that high CRIR values alleviate depletion effects.

We can also conclude from the results that it is critical to accurately assess the temperature of these cores at small scales, so more comprehensive temperature calculating schemes in similar conditions will be required in the future. It is important to note that our treatment of density-dependent temperature was quite simplistic, and it is very likely that it does not cover all of the effects on chemistry that a proper radiative transfer treatment of temperature would have.

To finalize, the results we obtained from properly modeling the 3D distribution of the gas show that there are cores where NH_3 is not depleting while its isotopologues are, in agreement with observational works. However, it is still an open question what is causing this chemical behavior, and further studies are needed to shed light on this specific point.

6.3 Future Prospects

Although the work done here is pretty intensive, we left, on purpose or not, some questions unanswered. This work can be expanded in multiple ways, such as by giving a review

to a set of non-isothermal cases that matches all the combinations of parameters used for isothermal cases, while also improving the density-dependence framework used here for variable temperature and/or looking for other easy-to-implement ones.

We can also further review the cases where deuterated ammonia isotopologues are present that were addressed quite superficially due to time and/or computational constraints. We point out that we may have left several cases out, and we would like to review them in the future if possible.

Bibliography

Aguti, E. D., Lada, C. J., Bergin, E. A., Alves, J. F., and Birkinshaw, M. (2007). "The Dynamical State fo the Starless Dense Core FeSt 1-457: A Pulsating Globule?" *arXiv e-prints*, arXiv:0705.0328.

Allamandola, L. J., Bernstein, M. P., Sandford, S. A., and Walker, R. L. (1999). "Evolution of interstellar ices." *Space Science Reviews*, *90*, 219–232.

Arata, S., Yajima, H., Nagamine, K., Abe, M., and Khochfar, S. (2020). "Starbursting [O III] emitters and quiescent [C II] emitters in the reionization era." , *498*(4), 5541–5556.

Bacmann, A., Lefloch, B., Ceccarelli, C., Castets, A., Steinacker, J., and Loinard, L. (2002). "The degree of CO depletion in pre-stellar cores." *Astronomy & Astrophysics*, *389*(1), L6–L10.

Bacmann, A., Lefloch, B., Ceccarelli, C., Steinacker, J., Castets, A., and Loinard, L. (2003). "CO Depletion and Deuterium Fractionation in Prestellar Cores." *The Astrophysical Journal*, *585*, L55–L58.

Bergin, E. A., Maret, S., van der Tak, F. F. S., Alves, J., Carmody, S. M., and Lada, C. J. (2006). "The thermal structure of gas in prestellar cores: A case study of barnard 68." *The Astrophysical Journal*, *645*(1), 369.

Bergin, E. A., and Tafalla, M. (2007). "Cold Dark Clouds: The Initial Conditions for Star Formation." *Annual Review of Astronomy and Astrophysics*, *45*(1), 339–396.

Bonnor, W. B. (1956). "Boyle's Law and Gravitational Instability." *Monthly Notices of the Royal Astronomical Society*, *116*(3), 351–359.

Bovino, S., Ferrada-Chamorro, S., Lupi, A., Sabatini, G., Giannetti, A., and Schleicher, D. R. G. (2019). "The 3D Structure of CO Depletion in High-mass Prestellar Regions." *The Astrophysical Journal*, *887*(2), 224.

Bovino, S., Ferrada-Chamorro, S., Lupi, A., Schleicher, D. R. G., and Caselli, P. (2020). "A new proxy to estimate the cosmic ray ionization rate in dense cores." *Monthly Notices of the Royal Astronomical Society: Letters*, *495*(1), L7–L11.

Bovino, S., Grassi, T., Schleicher, D. R. G., and Banerjee, R. (2016). "THE FORMATION OF THE PRIMITIVE STAR SDSS j102915172927: EFFECT OF THE DUST MASS AND THE GRAIN-SIZE DISTRIBUTION." *The Astrophysical Journal*, *832*(2), 154.

Brünken, S., Sipilä, O., Chambers, E. T., Harju, J., Caselli, P., Asvany, O., Honingh, C. E., Kamiński, T., Menten, K. M., Stutzki, J., and Schlemmer, S. (2014). "H_2D^+ observations give an age of at least one million years for a cloud core forming Sun-like stars." *Nature*, *516*(7530), 219–221.

Caselli, P., and Ceccarelli, C. (2012). "Our astrochemical heritage." , *20*, 56.

Caselli, P., Pineda, J. E., Sipilä, O., Zhao, B., Redaelli, E., Spezzano, S., Maureira, M. J., Alves, F., Bizzocchi, L., Bourke, T. L., Chacón-Tanarro, A., Friesen, R., Galli, D., Harju, J., Jiménez-Serra, I., Keto, E., Li, Z.-Y., Padovani, M., Schmiedeke, A., Tafalla, M., and Vastel, C. (2022). "The central 1000 au of a prestellar core revealed with ALMA. II. almost complete freeze-out." *The Astrophysical Journal*, *929*(1), 13.

Caselli, P., Stantcheva, T., Shalabiea, O., Shematovich, V. I., and Herbst, E. (2002a). "Deuterium fractionation on interstellar grains studied with modified rate equations and a Monte Carlo approach." *Planetary and Space Science*, *50*, 1257–1266.

Caselli, P., van der Tak, F. F. S., Ceccarelli, C., and Bacmann, A. (2003). "Abundant H2D+ in the pre-stellar core L1544." *Astronomy & Astrophysics*, *403*, L37–L41.

Caselli, P., Vastel, C., Ceccarelli, C., van der Tak, F. F. S., Crapsi, A., and Bacmann, A. (2008). "Survey of ortho-H2D+ (11,0-11,1) in dense cloud cores." *Astronomy & Astrophysics*, *492*(3), 703–718.

Caselli, P., Walmsley, M., Zucconi, A., Tafalla, M., Dore, L., and Myers, P. C. (2002b). "Molecular Ions in L1544. II. The Ionization Degree." *The Astrophysical Journal*, *565*(1), 344–358.

Cheung, A. C., Rank, D. M., Townes, C. H., Thornton, D. D., and Welch, W. J. (1968). "Detection of NH_3 Molecules in the Interstellar Medium by Their Microwave Emission." , *21*(25), 1701–1705.

Crapsi, A., Caselli, P., Walmsley, M., Myers, P. C., Tafalla, M., Lee, C. W., and Bourke, T. L. (2005). "Probing the Evolutionary Status of Starless Cores through N2H+ and N2D+ Observations." *The Astrophysical Journal*, *619*(1), 379–406.

Crapsi, A., Caselli, P., Walmsley, M. C., and Tafalla, M. (2007). "Observing the gas temperature drop in the high-density nucleus of l 1544." *Astronomy &amp Astrophysics*, *470*(1), 221–230.

Crutcher, R. M. (2012). "Magnetic Fields in Molecular Clouds." *Annual Review of Astronomy and Astrophysics*, *50*(1), 29–63.

Dame, T. M., Hartmann, D., and Thaddeus, P. (2001). "The milky way in molecular clouds: A new complete co survey." *The Astrophysical Journal*, *547*(2), 792–813.

Dame, T. M., Ungerechts, H., Cohen, R. S., de Geus, E. J., Grenier, I. A., May, J., Murphy, D. C., Nyman, L. A., and Thaddeus, P. (1987). "A Composite CO Survey of the Entire Milky Way." , *322*, 706.

Di Francesco, J., Evans, N. J., Caselli, P., Myers, P. C., Shirley, Y., Aikawa, A., and Tafalla, M. (2007). "An observational perspective of low-mass dense cores i: Internal physical and chemical properties."

Dislaire, V., Hily-Blant, P., Faure, A., Maret, S., Bacmann, A., and des Forê ts, G. P. (2011a). "Nitrogen hydrides and the hsub2/subortho-to-para ratio in dark clouds." *Astronomy &amp Astrophysics*, *537*, A20.

Dislaire, V., Hily-Blant, P., Faure, A., Maret, S., Bacmann, A., and Pineau Des Forêts, G. (2011b). "Nitrogen hydrides and the H2 ortho-to-para ratio in dark clouds." *Astronomy & Astrophysics*, *537*, 1–5.

Douglas, A. E., and Herzberg, G. (1941). "Note on CH$\hat{\{+\}}$ in Interstellar Space and in the Laboratory." , *94*, 381.

Draine, B. T. (2011). *Physics of the Interstellar and Intergalactic Medium*. Princeton University Press.

Draine, B. T., and Sutin, B. (1987). "Collisional charging of interstellar grains." *The Astrophysical Journal*, *320*(9), 803–817.

Federrath, C. (2016). "The role of turbulence, magnetic fields and feedback for star formation." *Journal of Physics: Conference Series*, *719*(1), 012002.

Fedoseev, G., Ioppolo, S., and Linnartz, H. (2015). "Deuterium enrichment of ammonia produced by surface N+H/D addition reactions at low temperature." *Monthly Notices of the Royal Astronomical Society*, *446*(1), 449–458.

Ferland, G. J., Korista, K. T., Verner, D. A., Ferguson, J. W., Kingdon, J. B., and Verner, E. M. (1998). "CLOUDY 90: Numerical Simulation of Plasmas and Their Spectra." , *110*(749), 761–778.

Ferrada-Chamorro, S., Lupi, A., and Bovino, S. (2021). "Chemical post-processing of magneto-hydrodynamical simulations of star-forming regions: robustness and pitfalls." *Monthly Notices of the Royal Astronomical Society*, *505*(3), 3442–3451.

Field, G. B., Goldsmith, D. W., and Habing, H. J. (1969). "Cosmic-ray heating of the interstellar gas." *The Astrophysical Journal*, *155*, L149.

Flower, D. R., Pineau des Forêts, G., and Walmsley, M. (2006). "The importance of the ortho:para H_2 ratio for the deuteration of molecules during pre-protostellar collapse." *Astronomy & Astrophysics*, *449*(2), 621–629.

Fontani, F., Busquet, G., Palau, A., Caselli, P., Sánchez-Monge, Á., Tan, J. C., and Audard, M. (2015). "Deuteration and evolution in the massive star formation process." *Astronomy & Astrophysics*, *575*, A87.

Fontani, F., Caselli, P., Crapsi, A., Cesaroni, R., Molinari, S., Testi, L., and Brand, J. (2006). "Searching for massive pre-stellar cores through observations of n2h$^+$ and n2d$^+$." *Astronomy & Astrophysics*, *460*(3), 709–720.

Fontani, F., Palau, A., Caselli, P., Sánchez-Monge, Á., Butler, M. J., Tan, J. C., Jiménez-Serra, I., Busquet, G., Leurini, S., and Audard, M. (2011). "Deuteration as an evolutionary tracer in massive-star formation." *Astronomy & Astrophysics*, *529*, L7.

Giannetti, A., Bovino, S., Caselli, P., Leurini, S., Schleicher, D. R. G., Körtgen, B., and Menten, K. M. (2019). "A timeline for massive star-forming regions via combined observation of o-H_2D^+ and N_2D^+." *Astronomy & Astrophysics*, *7*(621), 1–7.

Giannetti, A., Wyrowski, F., Brand, J., Csengeri, T., Fontani, F., Walmsley, M., Luong, Q. N., Beuther, H., Schuller, F., Güsten, R., and Menten, K. M. (2014). "ATLASGAL-selected massive clumps in the inner Galaxy: I. CO depletion and isotopic ratios." *Astronomy & Astrophysics*, *570*, 1–55.

Girart, J. M., Frau, P., Zhang, Q., Koch, P. M., Qiu, K., Tang, Y.-W., Lai, S.-P., and Ho, P. T. P. (2013). "DR 21(OH): A HIGHLY FRAGMENTED, MAGNETIZED, TURBULENT DENSE CORE." *The Astrophysical Journal*, *772*(1), 69.

Glover, S. C. O., Federrath, C., Mac Low, M. M., and Klessen, R. S. (2010). "Modelling co formation in the turbulent interstellar medium." *Monthly Notices of the Royal Astronomical Society*, *404*(1), 2–29.

Gnedin, N. Y., Tassis, K., and Kravtsov, A. V. (2009). "Modeling Molecular Hydrogen and Star Formation in Cosmological Simulations." , *697*(1), 55–67.

Grassi, T., Bovino, S., Haugbølle, T., and Schleicher, D. R. G. (2017). "A detailed framework to incorporate dust in hydrodynamical simulations." *Monthly Notices of the Royal Astronomical Society*, *466*(2), 1259–1274.

Grassi, T., Bovino, S., Schleicher, D. R. G., Prieto, J., Seifried, D., Simoncini, E., and Gianturco, F. A. (2014). "KROME - a package to embed chemistry in astrophysical simulations." *Monthly Notices of the Royal Astronomical Society*, *439*(3), 2386–2419.

Harju, J., Daniel, F., Sipilä, O., Caselli, P., Pineda, J. E., Friesen, R. K., Punanova, A., Güsten, R., Wiesenfeld, L., Myers, P. C., Faure, A., Hily-Blant, P., Rist, C., Rosolowsky, E., Schlemmer, S., and Shirley, Y. L. (2017). "Deuteration of ammonia in the starless core Ophiuchus/H-MM1." *Astronomy & Astrophysics*, *600*, A61.

Hasegawa, T. I., and Herbst, E. (1993). "New gas-grain chemical models of quiescent dense interstellar clouds: the effects of H2 tunnelling reactions and cosmic ray induced desorption." *Monthly Notices of the Royal Astronomical Society*, *261*, 83–102.

Heiles, C., and Crutcher, R. (2005). *Magnetic Fields in Diffuse HI and Molecular Clouds*, vol. 664, 137. Springer.

Herbst, E., Defrees, D. J., and McLean, A. D. (1987). "A Detailed Investigation of Proposed Gas-Phase Syntheses of Ammonia in Dense Interstellar Clouds." , *321*, 898.

Hidaka, H., Watanabe, M., Kouchi, A., and Watanabe, N. (2011). "Ftir study of ammonia formation via the successive hydrogenation of n atoms trapped in a solid n2 matrix at low temperatures." *Phys. Chem. Chem. Phys.*, *13*, 15798–15802.

Hily-Blant, P., Maret, S., Bacmann, A., Bottinelli, S., Parise, B., Caux, E., Faure, A., Bergin, E. A., Blake, G. A., Castets, A., Ceccarelli, C., Cernicharo, J., Coutens, A., Crimier, N., Demyk, K., Dominik, C., Gerin, M., Hennebelle, P., Henning, T., Kahane, C., Klotz, A., Melnick, G., Pagani, L., Schilke, P., Vastel, C., Wakelam, V., Walters, A., Baudry, A., Bell, T., Benedettini, M., Boogert, A., Cabrit, S., Caselli, P., Codella, C., Comito, C., Encrenaz, P., Falgarone, E., Fuente, A., Goldsmith, P. F., Helmich, F., Herbst, E., Jacq, T., Kama, M., Langer, W., Lefloch, B., Lis, D. C., Lord, S., Lorenzani, A., Neufeld, D., Nisini, B., Pacheco, S., Phillips, T., Salez, M., Saraceno, P., Schuster, K., Tielens, X., van der Tak, F. F. S., van der Wiel, M. H. D., Viti, S., Wyrowski, F., and Yorke, H. W. (2010). "Nitrogen hydrides in the cold envelope of IRAS 16293-2422." *Astronomy & Astrophysics*, *521*(L52), 3–9.

Ho, P. T. P., and Townes, C. H. (1983). "Interstellar ammonia." *Annual Review of Astronomy and Astrophysics*, *21*(1), 239–270.

Ivlev, A. V., Silsbee, K., Sipilä, O., and Caselli, P. (2019). "Gas and dust temperature in prestellar cores revisited: New limits on cosmic-ray ionization rate." *The Astrophysical Journal*, *884*(2), 176.

Jiménez-Serra, I., Vasyunin, A. I., Caselli, P., Marcelino, N., Billot, N., Viti, S., Testi, L., Vastel, C., Lefloch, B., and Bachiller, R. (2016). "The Spatial Distribution of Complex Organic Molecules in the L1544 Pre-stellar Core." , *830*(1), L6.

Katz, H., Kimm, T., Sijacki, D., and Haehnelt, M. G. (2017). "Interpreting ALMA observations of the ISM during the epoch of reionization." , *468*(4), 4831–4861.

Keating, L. C., Richings, A. J., Murray, N., Faucher-Giguère, C.-A., Hopkins, P. F., Wetzel, A., Kereš, D., Benincasa, S., Feldmann, R., Loebman, S., and Orr, M. E. (2020). "Reproducing the CO-to-H_2 conversion factor in cosmological simulations of Milky-Way-mass galaxies." , *499*(1), 837–850.

Keto, E., Rybicki, G. B., Bergin, E. A., and Plume, R. (2004). "Radiative transfer and starless cores." *The Astrophysical Journal*, *613*(1), 355.

Klessen, R. S., and Glover, S. C. O. (2016). "Physical processes in the interstellar medium." *Saas-Fee Advanced Course*, *43*, 85.

Kong, S., Caselli, P., Tan, J. C., Wakelam, V., and Sipilä, O. (2015). "The deuterium fractionation timescale in dense cloud cores: A parameter space exploration." *The Astrophysical Journal*, *804*(2).

Körtgen, B., Federrath, C., and Banerjee, R. (2019). "On the shape and completeness of the column density probability distribution function of molecular clouds." *Monthly Notices of the Royal Astronomical Society*, *482*(4), 5233–5240.

Krumholz, M. R. (2015). *Notes on Star Formation*. The Open Astrophysics Bookshelf.

Lada, C. J., and Lada, E. A. (2003). "Embedded Clusters in Molecular Clouds." *Annual Review of Astronomy and Astrophysics*, *41*(1), 57–115.

Larson, R. B. (1981). "Turbulence and star formation in molecular clouds." *Monthly Notices of the Royal Astronomical Society*, *194*, 809–826.

Le Bourlot, J. (1991a). "Ammonia formation and the ortho-to-para ratio of H2 in dark clouds." , *242*, 235.

Le Bourlot, J. (1991b). "Ammonia formation and the ortho-to-para ratio of H2 in dark clouds." , *242*, 235.

Le Gal, R., Hily-Blant, P., Faure, A., Pineau Des Forêts, G., Rist, C., and Maret, S. (2014). "Interstellar chemistry of nitrogen hydrides in dark clouds." *Astronomy & Astrophysics*, *562*, 1–20.

Lee, C. W., Myers, P. C., and Tafalla, M. (1999). "A survey of infall motions toward starless cores. i. CS (2–1) and nsub2/subhsup/sup(1–0) observations." *The Astrophysical Journal*, *526*(2), 788–805.

Lequeux, J. (2005). *The Interstellar Medium*. Astronomy and Astrophysics Library, Berlin, Heidelberg: Springer Berlin Heidelberg.

Linksy, J. L. (2003). "Atomic Deuterium/Hydrogen in the Galaxy." *Space Science Reviews*, *106*, 49–60.

Lique, F., Daniel, F., Pagani, L., and Feautrier, N. (2015). "Hyperfine excitation of n2h by h2: towards a revision of n2h abundance in cold molecular clouds." *Monthly Notices of the Royal Astronomical Society*, *446*(2), 1245–1251.

Lupi, A., and Bovino, S. (2020). "The [C II]-SFR correlation in dwarf galaxies across cosmic time." , *492*(2), 2818–2827.

Lupi, A., Bovino, S., Capelo, P. R., Volonteri, M., and Silk, J. (2018). "The natural emergence of the correlation between H_2 and star formation rate surface densities in galaxy simulations." , *474*(3), 2884–2903.

Lupi, A., Bovino, S., and Grassi, T. (2021). "On the low ortho-to-para H_2 ratio in star-forming filaments." , *654*, L6.

Lupi, A., Pallottini, A., Ferrara, A., Bovino, S., Carniani, S., and Vallini, L. (2020). "Predicting FIR lines from simulated galaxies." , *496*(4), 5160–5175.

Mathis, J. S., Rumpl, W., and Nordsieck, K. H. (1977). "The size distribution of interstellar grains." *The Astrophysical Journal*, *217*(2), 425.

McKee, C. F., and Ostriker, E. C. (2007). "Theory of Star Formation." *Annual Review of Astronomy and Astrophysics*, *45*(1), 565–687.

McKee, C. F., and Ostriker, J. P. (1977). "A theory of the interstellar medium - Three components regulated by supernova explosions in an inhomogeneous substrate." *The Astrophysical Journal*, *218*(9), 148.

Murray, N. (2011). "STAR FORMATION EFFICIENCIES AND LIFETIMES OF GIANT MOLECULAR CLOUDS IN THE MILKY WAY." *The Astrophysical Journal*, *729*(2), 133.

Nguyen, T., Baouche, S., Congiu, E., Diana, S., Pagani, L., and Dulieu, F. (2018). "Segregation effect and N_2 binding energy reduction in CO-N_2 systems adsorbed on water ice substrates." *Astronomy & Astrophysics*, *619*, A111.

Öberg, K. I., and Bergin, E. A. (2021). "Astrochemistry and compositions of planetary systems." , *893*, 1–48.

Padovani, M., Galli, D., and Glassgold, A. E. (2009). "Cosmic-ray ionization of molecular clouds." *Astronomy & Astrophysics*, *501*(2), 619–631.

Pagani, L., Vastel, C., Hugo, E., Kokoouline, V., Greene, C. H., Bacmann, A., Bayet, E., Ceccarelli, C., Peng, R., and Schlemmer, S. (2009). "Chemical modeling of L183 (L134N): an estimate of the ortho/para H_2 ratio." *Astronomy & Astrophysics*, *494*(2), 623–636.

Pallottini, A., Ferrara, A., Bovino, S., Vallini, L., Gallerani, S., Maiolino, R., and Salvadori, S. (2017). "The impact of chemistry on the structure of high-z galaxies." , *471*(4), 4128–4143.

Pallottini, A., Ferrara, A., Decataldo, D., Gallerani, S., Vallini, L., Carniani, S., Behrens, C., Kohandel, M., and Salvadori, S. (2019). "Deep into the structure of the first galaxies: SERRA views." , *487*(2), 1689–1708.

Pillai, T., Caselli, P., Kauffmann, J., Zhang, Q., Thompson, M. A., and Lis, D. C. (2012). "H_2D^+ in the high-mass star-forming region Cygnus-X." *The Astrophysical Journal*, *751*(2), 135.

Pineau des Forets, G., Roueff, E., and Flower, D. R. (1990). "The formation of nitrogen-bearing species in dark interstellar clouds." , *244*, 668–674.

Pineda, J. E., Harju, J., Caselli, P., Sipilä, O., Juvela, M., Vastel, C., Rosolowsky, E., Burkert, A., Friesen, R. K., Shirley, Y., Maureira, M. J., Choudhury, S., Segura-Cox, D. M., Güsten, R., Punanova, A., Bizzocchi, L., and Goodman, A. A. (2022). "An interferometric view of h-MM1. i. direct observation of NHsub3/sub depletion." *The Astronomical Journal*, *163*(6), 294.

Punanova, A., Caselli, P., Feng, S., Chacón-Tanarro, A., Ceccarelli, C., Neri, R., Fontani, F., Jiménez-Serra, I., Vastel, C., Bizzocchi, L., Pon, A., Vasyunin, A. I., Spezzano, S., Hily-Blant, P., Testi, L., Viti, S., Yamamoto, S., Alves, F., Bachiller, R., Balucani, N., Bianchi, E., Bottinelli, S., Caux, E., Choudhury, R., Codella, C., Dulieu, F., Favre, C., Holdship, J., Jaber Al-Edhari, A., Kahane, C., Laas, J., LeFloch, B., López-Sepulcre, A., Ospina-Zamudio, J., Oya, Y., Pineda, J. E., Podio, L., Quenard, D., Rimola, A., Sakai, N., Sims, I. R., Taquet, V., Theulé, P., and Ugliengo, P. (2018). "Seeds of Life in Space (SOLIS). III. Zooming Into the Methanol Peak of the Prestellar Core L1544." , *855*(2), 112.

Redaelli, E., Bizzocchi, L., Caselli, P., Sipilä, O., Lattanzi, V., Giuliano, B. M., and Spezzano, S. (2019). "High sensitivity maps of molecular ions in L1544: I. Deuteration of N2H+ and HCO+ and first evidence of N2D+ depletion." *Astronomy & Astrophysics*.

Redaelli, E., Bovino, S., Giannetti, A., Sabatini, G., Caselli, P., Wyrowski, F., Schleicher, D. R. G., and Colombo, D. (2021). "Identification of pre-stellar cores in high-mass star forming clumps via hsub2/subdsup/sup observations with ALMA." *650*, A202.

Richings, A. J., and Schaye, J. (2016). "Chemical evolution of giant molecular clouds in simulations of galaxies." , *460*(3), 2297–2321.

Richings, A. J., Schaye, J., and Oppenheimer, B. D. (2014). "Non-equilibrium chemistry and cooling in the diffuse interstellar medium - ii. shielded gas." *Monthly Notices of the Royal Astronomical Society*, *442*(3), 2780–2796.

Salpeter, E. E. (1955). "The luminosity function and stellar evolution." *The Astrophysical Journal*, *121*, 161.

Savage, B. D., Bohlin, R. C., Drake, J. F., and Budich, W. (1977). "A survey of interstellar molecular hydrogen. I." , *216*, 291–307.

Schnee, S., Caselli, P., Goodman, A., Arce, H. G., Ballesteros-Paredes, J., and Kuchibhotla, K. (2007). "TMC-1c: An accreting starless core." *The Astrophysical Journal*, *671*(2), 1839–1857.

Scott, G. B. I., Freeman, C. G., and McEwan, M. J. (1997). "The interstellar synthesis of ammonia." *Monthly Notices of the Royal Astronomical Society*, *290*(4), 636–638.

Shingledecker, C. N., Bergner, J. B., Gal, R. L., Oberg, K. I., Hincelin, U., and Herbst, E. (2016). "On the Inference of the Cosmic Ray Ionization Rate ζ from the HCO^+-to-DCO^+ Abundance Ratio: The Effect of Nuclear Spin." *The Astrophysical Journal*, *830*(2), 151.

Sipilä, O., Harju, J., Caselli, P., and Schlemmer, S. (2015). "Spin-state chemistry of deuterated ammonia." *Astronomy & Astrophysics*, *581*.

Sipilä, O., Hugo, E., Harju, J., Asvany, O., Juvela, M., and Schlemmer, S. (2010). "Modelling line emission of deuterated H3+ from prestellar cores." *Astronomy & Astrophysics*, *509*(1).

Sipilä, O., Caselli, P., Redaelli, E., Juvela, M., and Bizzocchi, L. (2019). "Why does ammonia not freeze out in the centre of pre-stellar cores?" *Monthly Notices of the Royal Astronomical Society*, *487*(1), 1269–1282.

Smith, I. W. W., Cockell, C. S., and Leach, S. (2013). *Astrochemistry and Astrobiology*. Berlin, Heidelberg: Springer Berlin Heidelberg.

Sohn, J., Lee, C. W., Park, Y.-S., Lee, H. M., Myers, P. C., and Lee, Y. (2007). "Probing inward motions in starless cores using the hcn(j = 1-0) hyperfine transitions: A pointing survey toward central regions." *The Astrophysical Journal*, *664*(2), 928.

Spilker, A. K. L. (2021). *Bird's-eye view of molecular clouds in the Milky Way*. Ph.D. thesis, Chalmers University of Technology, Sweden.

Suzuki, H., Yamamoto, S., Ohishi, M., Kaifu, N., Ishikawa, S.-I., Hirahara, Y., and Takano, S. (1992). "A survey of ccs, hc3n, hc 5n, and nh 3 toward dark cloud cores and their production chemistry." *The Astrophysical Journal*, *392*, 551.

Swings, P., and Rosenfeld, L. (1937). "Considerations Regarding Interstellar Molecules." *The Astrophysical Journal*, *86*, 483.

Tafalla, M., Myers, P., Caselli, P., and Walmsley, C. (2004). "On the internal structure of starless cores. physical and chemical properties of l1498 and l1517b." *Astrophysics and Space Science*, *292*(1-4), 347–354.

Tafalla, M., Santiago-García, J., Myers, P. C., Caselli, P., Walmsley, C. M., and Crapsi, A. (2006). "On the internal structure of starless cores. II. A molecular survey of L1498 and L1517B." , *455*(2), 577–593.

Tassis, K., Hezareh, T., and Willacy, K. (2012). "A SEARCH FOR CO-EVOLVING ION AND NEUTRAL GAS SPECIES IN PRESTELLAR MOLECULAR CLOUD CORES." *The Astrophysical Journal*, *760*(1), 57.

Tielens, X. (2005). *The Physics and Chemistry of the Interstellar Medium*. Cambridge.

Troscompt, N., Faure, A., Maret, S., Ceccarelli, C., Hily-Blant, P., and Wiesenfeld, L. (2009). "Constraining the ortho-to-para ratio of h_2 with anomalous h_2co absorption." *Astronomy & Astrophysics*, *506*(3), 1243–1247.

van Dishoeck, E. F. (2018). "Astrochemistry: overview and challenges." *IAU Symposium*, *332*, 3–22.

Vaytet, N., Tomida, K., and Chabrier, G. (2014). "On the role of the h_2 ortho:para ratio in gravitational collapse during star formation." *Astronomy & Astrophysics*, *563*, A85.

Wakelam, V., Loison, J.-C., Mereau, R., and Ruaud, M. (2017). "Binding energies: New values and impact on the efficiency of chemical desorption." *Molecular Astrophysics*, *6*, 22–35.

Walmsley, M., Flower, D. R., and Pineau des Forêts, G. (2004). "Complete depletion in prestellar cores." *Astronomy & Astrophysics*, *418*(3), 1035–1043.

Williams, J. P., Blitz, L., and McKee, C. F. (2000). "The structure and evolution of molecular clouds: from clumps to cores to the imf." In V. Mannings, A. P. Boss, and S. S. Russell (Eds.), *Protostars and Planets IV*, 97.

Yamamoto, S. (2003). *Introduction to Astrochemistry*. Springer Berlin Heidelberg.

Yoshida, N. (2019). "Formation of the first generation of stars and blackholes in the universe." *Proceedings of the Japan Academy, Series B*, *95*, 17–28.

Ysard, N., Köhler, M., Jones, A., Dartois, E., Godard, M., and Gavilan, L. (2016). "Mantle formation, coagulation, and the origin of cloud/core shine." *Astronomy &amp Astrophysics*, *588*, A44.